Unusual marbles in a non-metamorphic succession of the SW Alps (Valdieri, Italy) due to early Oligocene hydrothermal flow

Unusual marbles in a non-metamorphic succession of the SW Alps (Valdieri, Italy) due to early Oligocene hydrothermal flows

Carlo Bertok[1*], Luca Barale[2], Anna d'Atri[1,2], Luca Martire[1], Fabrizio Piana[2], Piergiorgio Rossetti[1], Axel Gerdes[3]

[1] Dipartimento di Scienze della Terra, Università di Torino, via Valperga Caluso 35, 10125 Turin, Italy

[2] CNR IGG – Torino, via Valperga Caluso 35, 10125 Turin, Italy

[3] Department of Geosciences, Goethe University Frankfurt, 60438 Frankfurt am Main, Germany

[*]Corresponding author. Email: carlo.bertok@unito.it

ORCiD
Carlo Bertok: http://orcid.org/0000-0001-9793-8078
Luca Barale: http://orcid.org/0000-0002-8493-1974
Anna d'Atri: http://orcid.org/0000-0002-3560-1610
Luca Martire: http://orcid.org/0000-0002-7765-0269
Fabrizio Piana: http://orcid.org/0000-0001-7049-3160
Piergiorgio Rossetti: http://orcid.org/0000-0002-0269-1330
Axel Gerdes: https://orcid.org/0000-0003-3823-2125

Abstract

In the SW Alps, at the NE margin of the Argentera Massif, the occurrence of isolated bodies of silicate-bearing marbles (Valdieri Marble), laterally passing to non-metamorphic Mesozoic limestones of the Dauphinois succession, appears enigmatic, since their origin can not be related to the regional metamorphism. The stratigraphic, geometric, petrographic, and geochemical features of the Valdieri Marble indicate that it originated from the upflow of hydrothermal fluids which deeply recrystallised the limestone and provoked the abundant neoblastesis of silicate minerals, at an estimated crystallisation temperature of ca. 350 °C.

This paper provides for the first time an absolute U/Pb age, comprised between 30 and 31.6 Ma (early Oligocene), for the Valdieri Marble, which is affected by a syn-genetic shear foliation in turn crosscut by the main Alpine tectonic foliations.

The hydrothermal fluids that formed the Valdieri Marble migrated along low-angle shear zones, mostly parallel to the sedimentary primary bedding, which were downward connected with high-angle master faults of the “Alpine SW transfer”, a main Oligocene-early Miocene transcurrent shear zone at the southern termination of the Western Alps. The localized heat flow sustaining the hydrothermal system could be related to the early Oligocene thermal event, well documented by magmatic activity in the Western and Central Alps.

Keywords: Valdieri Marble; Dauphinois Domain; Maritime Alps; U/Pb geochronology; Hydrothermal flows; Alpine SW transfer

1 Introduction

The recognition of fossil hydrothermal systems provides precious information on the tectono-stratigraphic evolution of geological units, documenting extensional or transtensional tectonics possibly associated with geothermal anomalies, and becomes crucial in orogenic settings, where younger compressive tectonics commonly reactivated and overprinted preexisting faults and fractures (e.g.: Barale et al., 2016b; Incerpi et al., 2017). Here

hydrothermal products thus represent the only evidence for such phenomena; however, they have probably often been overlooked in the past, partly because of the difficulty to distinguish them from the effects of the regional metamorphism. Carbonate sedimentary successions are a favourable target to record hydrothermal fluxes, because of their tendency to recrystallize and to host diagenetic minerals (e.g.: hydrothermal dolomite, Davies and Smith 2006; Barale et al., 2016b). Unfortunately, they often lack radiogenic minerals suitable for the most commonly used radiometric dating methods, thus commonly impeding to precisely date the related hydrothermal events and to understand their significance for the regional tectono-stratigraphic evolution. The recent advances in the U/Pb datings of carbonates, however, provide a powerful tool to overcome this limitation, and push to reconsider some lithological “anomalies”, particularly those occurring in the external sectors of the Alps, where the regional metamorphism never exceeded anchizonal conditions.

In the Maritime Alps, at the northeastern margin of the Argentera Massif, hundreds of metres-size bodies of silicate-bearing marbles (known as "Valdieri Marble") are included in the Mesozoic stratigraphic succession of the Dauphinois Domain. The Valdieri Marble was derived from localized recrystallisation of Cretaceous, mainly carbonate lithostratigraphic units (Lausa Limestone, Marne Nere, Puriac Limestone).

The Valdieri Marble has been known for a long time as a valuable ornamental stone (e.g., Mendes da Costa 1757; Nicolis de Robilant 1786; Albanis Beaumont 1795; Barelli 1835; Sismonda 1833, 1848; Franchi 1926; Malaroda 1957; Catella 1965, 1969; Carraro et al. 1970; Fornaro et al. 2005). Nowadays, the Valdieri Marble is no more exploited as an ornamental stone; it is still extracted in the San Lorenzo quarry by Carbocalcio Cuneese Spa to produce marble granulates and powders for industrial uses.

However, the origin of these rocks was not investigated in detail, and their significance in the frame of the geological evolution of the Maritime Alps has never been discussed. Their occurrence as isolated bodies within a carbonate succession showing very low

recrystallisation and unaffected by neoblastic growth of silicate minerals sounds unusual and the relationships with regional metamorphism appear to be not so straightforward.

This paper provides new data collected through detailed field surveys, petrographic, geochemical and geochronological studies, in order to pursue four main goals:

- to describe in detail the field and petrographic features of the Valdieri Marble, as well as the relationships among marble bodies and the adjoining, poorly-recrystallised stratigraphic successions;
- to investigate the genetic processes of these marbles;
- to present new U/Pb geochronological data, which very consistently provide the age of formation of the Valdieri Marble;
- to discuss the geodynamic meaning of the origin of the Valdieri Marble in the context of the geological evolution of the SW Alps.

2 Geological setting

The Valdieri Marble crops out between the Gesso and lower Stura valleys (Maritime Alps, NW Italy), at the north-eastern boundary of the Argentera Massif, within the Entracque Unit (d'Atri et al. 2016) (Figs. 1, 2). The Entracque Unit is part of the Dauphinois-Provençal Domain, which corresponds to the proximal portion of the Mesozoic Alpine Tethys European palaeomargin. The area was mapped at 1:100,000 by Abiad et al. (1970), at 1:50,000 by Malaroda (1970), and more recently by Barale et al. (2016a) at 1:25,000 scale. The stratigraphic succession of the Entracque Unit starts with Lower Triassic continental to coastal deposits, resting on the crystalline basement of the Argentera Massif. They are followed by Middle Triassic peritidal carbonates, Upper Triassic continental shales, Rhaetian–Hettangian peritidal carbonates, and Sinemurian, open-platform bioclastic limestones (Carraro et al. 1970; Barale et al. 2016a). Since the Early–Middle Jurassic, the northwestern sector of the Entracque Unit evolved as a subsiding basin with a Dauphinois type succession characterized by thick hemipelagic–pelagic deposits (Malaroda 1963; Carraro et al. 1970; Barale et al. 2016a, 2017). The succession starts with Middle? Jurassic–

Berriasian? dark marls and shales (Entracque Marl) and Valanginian?–early Aptian? pelagic limestones (Lausa Limestone), both containing resedimented carbonate breccia beds. In the Lausa Limestone, clasts and, locally, m-sized blocks of coarsely-crystalline dolostone, possibly derived from hydrothermally dolomitized Jurassic platform carbonates of the adjoining Provençal Domain (Barale et al. 2016a, b), occur. The succession continues with Aptian–Cenomanian marls (Marne Nere) and a thick Turonian p.p.–Campanian marly limestone succession (Puriac Limestone), containing two detrital lithozones. The first one, in the lower part of the unit, contains cm- to dm-thick beds of packstones with reworked dolomite grains, whereas the second one, in the upper part of the unit, contains cm- to dm-thick beds of lithoarenites and sandy limestones mainly composed of siliciclastic grains (Carraro et al. 1970; Bersezio et al. 2002; Barale et al. 2017).

The top of the Mesozoic succession is truncated by a regional unconformity, corresponding to a hiatus spanning the latest Cretaceous–middle Eocene, overlain by the Alpine Foreland Basin succession. It consists of Lutetian? - early Bartonian discontinuous continental clast-supported conglomerates (*Microcodium* Formation), followed by Bartonian - early Priabonian shallow water nummulitid-bearing sandy limestones (Nummulitic Limestone). The Nummulitic Limestone is topped by upper Eocene hemipelagic foraminifera-rich calcareous marls (*Globigerina* Marl), in turn overlain by late Priabonian–early Oligocene turbidite sandstones and shales (Grès d'Annot).

Starting from the late Oligocene, the Entracque Unit experienced at least three phases of Alpine deformation: (i) southwestward brittle-ductile thrusting and superposed folding, (ii) northeastward back-vergent folding, and (iii) southward brittle thrusting and flexural folding (d'Atri et al. 2016, and reference therein). The regional kinematic setting was achieved in the frame of a transpressional regime with important strain partitioning of contractional and strike-slip-related structural associations (Piana et al. 2009; d'Atri et al. 2016), as evidenced by the occurrence of a late-Oligocene-Miocene NW–SE Alpine transcurrent shear zone (Limone–Viozene Zone), running for several kilometres SE of the Gesso Valley, and of the E–W strike-slip Demonte–Aisone shear zone in the lower Stura Valley (d'Atri et al. 2016).

Based on illite and chlorite crystallinity indices (KI, AI) for adjoining tectonic units, Piana et al. (2014) inferred very low Alpine metamorphic conditions (middle anchizone), and it is reasonable to assume similarly low metamorphic grades for the entire Entracque Unit. The local conversion of anchizonal limestones and marls (from the upper part of the Entracque Marl to the Puriac Limestone) to greenschist facies marble (the Valdieri Marble) is thus problematic. This paper presents a detailed description of the marbles and their petrography, mineral chemistry and age, to provide an explanation for this unusual and peculiar lithological occurrence.

3 Materials and methods

Detailed field surveys were performed in order to investigate stratigraphic and structural features of the Valdieri Marble, and its geometric relationships with the surrounding sedimentary rocks. An extensive sampling was accomplished in order to carry out a thorough petrographic study by optical and electron microscopy, to characterize minerochemical features of the Valdieri Marble, and to provide a radiometric dating of its formation.

3.1 Mineral chemistry

In situ quantitative microprobe analyses were performed on carbon-coated polished-thin sections with a Cambridge Stereoscan 360 and with a JEOL JSM-IT300LV SEM equipped with an EDS Energy 200 and a Pentafet detector (Oxford Instruments) at the Department of Earth Sciences, University of Torino. The operating conditions were 50 s counting time and 15 kV accelerating voltage. SEM–EDS quantitative data (spot size = 2 μm) were acquired and processed using the Microanalysis Suite Issue 12, INCA Suite version 4.01; natural mineral standards were used to calibrate the raw data.

3.2 U/Pb dating

Uranium-lead ages were acquired in situ on polished thin section of marbles from seven different samples (Fig. SM2 in the Supplementary Material) by laser ablation-inductively coupled plasma-mass spectrometry (LA-ICP-MS) at the Goethe University Frankfurt (GUF), using a method modified by Gerdes and Zeh (2006, 2009). Recent studies have shown that this method yields precise and accurate ages on carbonate formed during different processes (Li et al. 2015; Coggan et al. 2015; Ring and Gerdes 2016; Mettner et al. 2016; Hansman et al. 2018). At GUF a Thermo Scientific Element 2 sector field ICP-MS is coupled to a Resolution S-155 (Resonetics) 193 nm ArF Excimer laser (CompexPro 102, Coherent) equipped with a two-volume ablation cell (Laurin Technic, Australia). Samples were ablated in a helium atmosphere (0.6 l/min) and mixed in the ablation funnel with 0.7 l/min argon and 0.04 l/min nitrogen. Signal strength at the ICP-MS was tuned for maximum sensitivity while keeping oxide formation below 0.3% (UO/U). Static ablation used a spot size of 213 µm and a fluence of < 1 J cm^{-2} at 6 Hz. This yielded for SRM-NIST 614 a depth penetration of about 0.5 µm s^{-1} and an average sensitivity of 420000 cps/µg g^{-1} for ^{238}U. The detection limits for ^{206}Pb and ^{238}U were ~ 0.1 and 0.03 ppb, respectively. However, at a U signal of less 1000 cps (~ 2 ppb) the data were generally discarded due to enhanced scatter on the isotope ratios.

Data were acquired in fully-automated mode overnight during two independent analytical sessions (2014 and 2015) in sequences of 388 to 598 analyses. Each analysis consists of 20 s background acquisition followed by 20 s of sample ablation and 25 s washout. During 42 s data acquisition, the signals of ^{206}Pb, ^{207}Pb, ^{208}Pb, ^{232}Th and ^{238}U were detected by peak jumping in pulse counting mode with a total integration time of 0.1 s, resulting in 420 mass scans. Prior to analysis each spot was pre-ablated for 3 s to remove surface contamination. Soda-lime glass SRM-NIST 614 was used as a reference glass together with 2 carbonate standards to bracket sample analysis.

Raw data were corrected offline using an in-house MS Excel© spread-sheet program (Gerdes and Zeh 2006, 2009). Following background correction, outliers (±2σ, standard deviation) were rejected based on the time-resolved $^{207}Pb/^{206}Pb$ and $^{206}Pb/^{238}U$ ratios. The

$^{207}Pb/^{206}Pb$ ratio was corrected for mass bias (0.3%) and the $^{206}Pb/^{238}U$ ratio for inter-element fraction (ca. 5%), including drift over the 12 hours of sequence time, using SRM-NIST 614. Due to the carbonate matrix an additional correction of 3% has been applied on the $^{206}Pb/^{238}U$, which was determined using WC-1 carbonate reference material dated by TIMS (254.4; Roberts et al. 2017). 34 runs of the WC-1 carbonate standard over the course of the two analytical sessions provided a lower intercept age of 254.1±1.1 Ma (2σ). Repeated analyses (n=35) of a Zechstein dolomite (255±4 Ma; Gypsum pit, Tettenborn, Germany) used as secondary (in-house) standard yielded a lower intercept age of 256.0 ± 2.0 Ma (MSWD: 1.3), implying an accuracy and repeatability of the method of around 2% or better. The analytical results are presented in Table SM1, provided in the Supplementary Material. Data were plotted in the Tera-Wasserburg diagram and ages calculated as lower intercepts using Isoplot 3.71 (Ludwig 2007) (Fig. SM3 in the Supplementary Material). All uncertainties are reported at the 2σ level.

4 Distribution and geometry of the marble bodies

The Valdieri Marble occurs in two irregularly shaped, hundreds of metres- to kilometre-sized bodies located in the southern side of Monte La Piastra (San Lorenzo quarry Figs. 1, 2, 3), and in the sector extending from the upper Desertetto Valley (Desertetto quarries) to the northern side of Cima Cialancia (Cima Cialancia quarry) (Figs. 1, 2). In the Desertetto valley-Cima Cialancia sector the recrystallisation affected the succession up to the upper part of the Puriac Limestone, whilst in the San Lorenzo quarry the recrystallisation is limited to the lower part of the Puriac Limestone, not involving the upper one. In the marble bodies the original sediments were irregularly affected by a very intense recrystallisation, giving rise to the growth of medium to very coarsely crystalline calcite and new silicate minerals. This resulted in a complete obliteration of the primary features of the limestones, and in the development of the metamorphic Valdieri Marble. The main marble bodies transitionally pass, over a distance of a few tens of metres, to the carbonate rocks of the corresponding lithostratigraphic units, which are characterized by a very slight recrystallisation of the

carbonate fraction, transformed in microsparitic calcite, whereas the terrigenous fraction is unaffected by recrystallisation and no neoblastic minerals are present (Fig. 4a). Rocks occurring in the transition zone show strongly variable recrystallisation degrees of the carbonate fraction, even at a centimetre scale, and a neoblastesis of fine-grained white mica locally occurring in the terrigenous fraction.

5 Petrographic and compositional features

A description of Valdieri Marble is provided here, following the stratigraphic order of the original lithostratigraphic units. In section 5.1 petrographic and compositional features of the marbles originated from the Lausa Limestone (hereafter referred to as “San Lorenzo Marble”), are reported. Sections 5.2 and 5.3 are dedicated to the marbles derived from the recrystallisation of the overlying Marne Nere and Puriac Limestone units (hereafter called “recrystallised Marne Nere” and “Desertetto Marble”, respectively). The recrystallised Entracque Marl has not been described since it is observable only in one small outcrop, showing similar features to the S. Lorenzo Marble. In section 5.4 different types of veins crosscutting the marble bodies are described, and in section 5.5 possible constraints to P-T conditions of recrystallisation are discussed.

5.1 San Lorenzo Marble

The San Lorenzo Marble, well exposed in the San Lorenzo quarry, is mainly represented by white to grey marbles, –locally banded, consisting of granoblastic calcite associated with very minor white mica and quartz (Fig. 4b). Yellowish-brown, mm- to cm- sized clasts and, locally, dm- to m-sized blocks made of coarsely crystalline dolostones, occur within the marbles. They most probably correspond to dolomite clasts and blocks resedimented from the Provençal Domain during the sedimentation of the Lausa Limestone, as documented by Barale et al. (2016a, 2017). Both white mica (as fine-grained lepidoblasts) and dolostone clasts are oriented to define a foliation (Fig. 4c, d). Locally, within the pure marble, cm-thick, elongated portions occur, light brown in color, rich in muscovite, K-feldspar, albite and

quartz. These portions are composed of alternating domains strongly enriched, alternatively, in K-feldspar, white mica ± pyrite, or K-feldspar + albite, quartz and calcite (Fig. 5). This banded texture is strongly folded, and centimetre-sized hinges are well visible also at the microscale. The K-feldspar is mostly concentrated along thin (some hundred microns thick) layers, as 500-2000 μm long elongated crystals, often surrounded by white mica + pyrite and calcite; feldspar crystals, elongated parallel to the rock foliation, are broken and re-oriented by folding (Fig. 5a, b). K-feldspar contains abundant oriented inclusions of phyllosilicates, which suggest growth over a pre-existing foliation. In some domains, albite also occurs (Fig. 5c), as euhedral crystals up to 300 μm long often enclosed by K-feldspar. The albite crystals locally show the “Roc Tourné twinning”, a feature typically displayed by authigenic albite (Kastner 1971) and commonly observed in the Valdieri–Entracque area in different stratigraphic intervals (mainly within the Marne Nere and Puriac Limestone) (Barale 2014). Albite is always pure and K-feldspar shows a very low content (≤ 4%) of the Ab component. The white mica is often concentrated in domains, alone or associated with very fine-grained pyrite and locally albite. It shows a muscovite composition characterized – compared with the Desertetto Marble– by relatively high Si and Mg contents (3.2-3.4 and 0.2-0.4 apfu respectively: see Fig. 8b; Fig. SM1 in the supplementary material).

The foliated domains abruptly terminate laterally against granoblastic calcite intergrowths (Fig. 5d). As in the Desertetto Marble (see below), such calcite intergrowths – which unequivocally postdate the deformed foliation - are not related to veins. Rather, they are related to anastomosing to cloud-like carbonate pockets which were probably formed by diffusive fluid flow.

5.2 Recrystallised Marne Nere

In the eastern side of San Lorenzo quarry an about 8 metres-thick interval of calcareous schists, derived from the recrystallisation of the Marne Nere, occurs in stratigraphic contact with the underlying San Lorenzo Marble (Figs. 3, 6a). These rocks show a porphyroclastic structure, with large calcite crystals (probably echinoderm fragments) enveloped by the

foliation. The latter is given by the alternation of domains strongly enriched in calcite or white mica and chlorite (Fig. 6b). The micaceous domains also contain very fine grained pyrite and dark carbonaceous material. Detrital quartz grains, 20-100 μm in diameter, are locally present.. Albite and pyrite are common accessory minerals, both forming euhedral crystals with no apparent relation with the rock foliation. Some thin, laterally discontinuous beds with abundant preserved echinoderm fragments have been interpreted as the equivalent of lenticular beds of echinoderm-rich packstones locally occurring in the Marne Nere in the Entracque area (Barale, 2014; Barale et al., 2017).

5.3 Desertetto Marble

The Desertetto Marble is well exposed in the area between the upper Desertetto valley and the Cima Cialancia abandoned quarry. In the upper Desertetto Valley, the recrystallized Marne Nere are overlain by 20-30 meters of banded white and grey marbles with rare phyllosilicate levels, followed by 15-20 meters of white marbles with millimeter-sized dolostone clasts, corresponding to the first detrital lithozone with reworked dolomite clasts and grains described by Barale et al. (2017) in the lower portion of the Puriac Limestone. The succession continues with an interval of silicate-bearing marbles, which was quarried in the past in the Cima Cialancia and Desertetto quarries. It is composed of lens-shaped, cm- to dm-thick white marble portions interlayered with mm-thick anastomosing greenish to purple levels, locally giving rise to a breccia texture (Figs. 6c,d). The white domains consist of a completely recrystallised, mostly isotropic granoblastic calcite intergrowth. The greenish domains are instead mainly composed of white mica and epidote, with minor chlorite and calcite (Fig. 7a). White mica is strongly iso-oriented to define a foliation parallel to the domain margins, and locally strongly folded. Epidote can be abundant and occurs as subhedral crystals up to few millimeters long, mostly synkinematic with respect to the host foliation (Fig. 7c); they often show a dark core of very fine-grained hematite. Post-kinematic epidote also occurs, which overgrows the deformed foliation (Fig. 7d). Synkinematic epidote is an epidote-clinozoisite solid solution spanning a relatively wide composition range (Ep_{58} to

Ep_{98}: Fig. 8a) and often showing a weak zoning, the rims being slightly enriched in the Ep component (e.g., Ep_{65} to Ep_{64}). Post-kinematic epidote is also an epidote-clinozoisite solid solution, displaying a restricted composition range (Ep_{69} to Ep_{76}, Fig. 8a). In certain white mica + epidote domains, the epidote may contain abundant small patches (few microns across: Fig. 9a) strongly enriched in LREE (La_2O_3+Ce_2O_3+Nd_2O_3 up to ~13 wt%) and Th (ThO_2 up to ~2.8 wt%). The irregular shape of the REE-rich patches, coupled with their concentration within certain domains, suggests that they represent pre-metamorphic relics of allanitic epidote (see below). Only rarely, the rare earth enrichments match crystal zoning (Fig. 9b), thus suggesting that some REE redistribution occurred during the epidote growth. The domains which contain epidotes showing REE enrichments also contain abundant detrital apatite, titanite, zircon, tourmaline and rutile grains as inclusions in white mica and epidote.

The white mica in the foliated domains is a muscovite-paragonite solid solution spanning a wide composition range, from almost pure muscovite (Mu_{91}) to paragonite-rich terms (Pa_{85}) (Fig. 8b); the margarite component is absent to very low (generally <5%). Both the muscovite- and paragonite-rich terms occur together within the same domain, as oriented lepidoblasts. As shown in the Si vs. K/K+Na diagram of Fig. 8b, several analyses show an intermediate composition. This could be due to the existence of an intermediate micaceous phase, or rather to very fine-grained muscovite-paragonite intergrowths (see Giorgetti et al. 2003, with refs.), as suggested by BSE observations. Chlorite (ripidolite to pycnochlorite: Fig. 10) also occurs, as lepidoblasts parallel to the foliation, at least locally in apparent equilibrium relationships with the white mica. Within the same domains, a second mica generation is represented by Mu-rich ($Mu_{84\text{-}89}$), randomly oriented lepidoblasts overgrowing the deformed foliation (Fig. 11a). The contact between the micaceous and the marble domains is commonly marked by the interposition of a mm-thick rim composed of an intergrowth of calcite, white mica and chlorite. In these domains the white mica is rich in muscovite ($Mu_{79\text{-}90}$) and mostly occurs as randomly oriented, relatively coarse-grained flakes (up to 300 μm long) showing equilibrium relationships with both calcite and chlorite (Figs. 7b,

11b). Chlorite shows sharp contacts with the white mica and shows a restricted composition range, falling in the ripidolite field (Fig. 10). Some late chlorite also occurs at rims of white mica, and likely represents a retrogression product. The Mu-rich lepidoblasts can show a paragonitic rim (Pa_{59-87}), which also is likely related to retrogression.

In the eastern side of the San Lorenzo quarry, the base of the Desertetto Marble (Figs. 3, 6a) is composed of impure white to grey marbles showing an intermediate degree of recrystallisation between the completely recrystallised Desertetto Marble outcropping in the upper Desertetto valley and the unaffected Puriac Limestone. These marbles are composed of interbedded domains alternatively enriched in carbonate or white mica. The carbonate domains consist of granoblastic calcite with minor neoblastic white mica and quartz, the latter as isolated rounded grains or polycrystalline aggregates after clastic quartz (Fig. 12a). Albite crystals showing “Roc Tourné twinning” also occur, in equilibrium with granoblastic calcite. The micaceous domains are composed of neoblastic muscovite (Mu_{100}), oriented along a foliation which envelops abundant relics of detrital plagioclase (showing polysynthetic twinning) and K-feldspar clasts, partially sericitized (Figs. 12b,c). Abundant titanite, rutile, zircon, monazite and tourmaline, all of them of clearly detrital origin, occur in some micaceous domains (Fig. 12d). The alternation of carbonate and micaceous domains and the abundance of accessory phases in certain micaceous horizons are striking analogies with the completely recrystallized Desertetto Marble of the upper Desertetto valley. A further increase of the degree of recrystallisation would have likely produced the complete destruction of feldspar: particularly, the breakdown of the albitic plagioclase could easily explain the formation of paragonitic mica.

5.4 Veins

Several types of veins occur, with different features, in all the marble units.

S. Lorenzo Marble: the S. Lorenzo Marble is crosscut by dm-thick, sub-vertical veins, filled with calcite (Fig. 13a). Calcite is often coarse-grained, as euhedral crystals up to 2 cm

across, slightly deformed and overgrown by fine grained calcite along microcracks; it is associated with very minor mica and quartz.

Networks of cm-thick veins are found in dolostone blocks occurring in the lower part of the S. Lorenzo Marble (Fig. 13b). These veins are mostly composed of calcite and a variable amount of quartz, the latter often occurring as euhedral crystals projecting from the vein walls; brownish Fe-bearing carbonate (presently altered to calcite + Fe hydroxide) and rare muscovite may also occur. The host dolostone is apparently not affected by recrystallisation; on the contrary, dolomite is clearly recrystallised when occurring as millimetre-sized dolostone clasts within the veins.

Recrystallised Marne Nere: veins crosscutting the recrystallised Marne Nere are irregularly shaped and show a variable thickness, ranging -even along the same vein- from centimetre to decimetre. They are mainly composed of quartz and calcite, with local concentrations of muscovite lepidoblasts, generally representing wallrock inclusions. An Fe-bearing carbonate, strongly weathered to Fe-hydroxides, may also occur in equilibrium relationships with calcite.

Desertetto Marble: in the eastern side of the San Lorenzo quarry, the lower part of the Desertetto Marble is crosscut by a few irregularly shaped veins, up to ca. 30 cm thick, filled with coarse-grained calcite and quartz cements. In the upper Desertetto valley, where the degree of recrystallisation is much stronger, the marble foliation is cut by irregularly-shaped pockets devoid of lateral continuity (Fig. 13c) and composed of calcite and epidote (Fig. 13d) (epidote-clinozoisite s.s. Ep_{57-84}: Fig. 11a), with localized white mica (muscovite-paragonite s.s., Mu_{79-87}: Fig. 11b) enrichments.

5.5 Constraints to the T-P conditions of recrystallisation

The determination of T-P conditions of recrystallisation is not straightforwardbecause the more significant assemblages occur within domains characterized by unusual compositions (i.e., the muscovite-paragonite ss. + epidote of the Desertetto Marble is restricted to portions with strong enrichments in Al and Na).

Geothermometric estimates for the Desertetto Marble, based on the T dependence of the K–Na partitioning in muscovite-paragonite pairs (e.g., Blencoe et al., 1994; Guidotti et al., 1994), are not reliable, due to the wide composition range likely due to the occurrence of sub-microscopic two-phase intergrowths.

An attempt to obtain indications on the recrystallisation temperature can be made with the "chlorite geothermometer", based on the relationship between T and Al^{IV} in chlorite (Chatelineau, 1988). The geothermometer has been applied to the chlorite (ripidolite - pycnochlorite) which occurs, in textural equilibrium with white mica and calcite, along the contact between micaceous and calcitic domains in the strongly recrystallised Desertetto Marble. Several other calibrations of this geothermometer occur, aimed at considering also the effects of the Fe-Mg substitution, pH and other factors (Walshe, 1986; Kranitiotis & McLean, 1987; Zang and Fyfe, 1995). We chose to apply the Chatelineau (1988) calibration, because *i)* it applies to chlorite where Σ[Ca + Na + K] <0.2 apfu, *ii)* was empirically calibrated at low P (Los Azufres geothermal system), *iii)* is probably the most appropriate for hydrothermal or metamorphic chlorite with $X_{Fe} < 0.5$ (Frimmel, 1997).

The crystallisation temperatures calculated for the Desertetto Marble vary from 304 to 363 °C, with most values around 350°C (avg. T = 355°C). These T estimates appear consistent with the observed metamorphic assemblage, particularly with the occurrence of epidote + paragonitic mica in the Desertetto Marble.

6 Structural features

6.1 Marble-host rock interface

No tectonic structures such as fractures, veins or shear zones have been observed at the boundary between the Valdieri Marble bodies and the primary carbonate host rocks, which, on the contrary, always corresponds to a transitional contact, characterized by a gradual decrease in the recrystallization degree and occurrence of neoblastic minerals.

6.2 Tectonic foliation formed during the marble formation

The Valdieri Marble shows an internal foliation, mostly parallel to the primary bedding, which can be appreciated both at the micro- and meso scale (labelled as Sm in the inset of Fig. 14). At the microscale the foliation is defined, both in the Desertetto Marble and in the impure portions of the San Lorenzo Marble, by the alternation of carbonate-rich domains and darker phyllosilicate- and/or K-feldspar-rich domains, to depict a banded texture (Figs. 7 and 5). The microscale foliation is folded, locally sheared and clearly overgrown by younger mineral grains (such as epidote in Figs. 7c and d), which demonstrates that blastesis occurred during and after the development of the foliation and its shearing. At the mesoscale the foliation can be perceived due to the mm- to cm-scale alternation of elongated carbonate domains or levels (locally punctuated by dolostone clasts), with thinner phyllosilicate levels (Figs. 4d, 6c,d, 15a). This foliation is strongly deformed by centimetre-sized folds (Fig. 15b), which are mostly similar folds formed under a shearing regime, locally giving rise to a shearing foliation (labelled as Sm_sh in Figs. 14 and 15b). These folds, which are only locally preserved, do not show any genetic relations with the more recent, large F2 folds that widely occur in the left side of the Gesso valley, where the Valdieri Marble quarries are located (Figs. 1c, 2, 3). As discussed below, these old similar folds probably originated under a local stress regime coeval with the hydrothermal fluid circulation that drove the metamorphism of limestone into marble.

6.3 Tectonic foliations formed after the marble formation, and related macroscale folds and fault systems.

The Valdieri Marble and its internal foliation are cross-cut by at least two generations of subsequent tectonic foliations, which can be both correlated with the main Alpine regional foliations occurring throughout the Entracque Unit (Fig. 14).

- The older among the Alpine regional foliations (labelled as S2 in Fig. 14) is a mm- to cm-spaced dissolution cleavage that occurs preferentially in the axial zone of some large scale

open folds belonging to a ENE-WSW fold system widely developed in the left side of the Gesso valley (F2 regional tectonic event sensu d'Atri et al., 2016). This fold system, characterised by open to close folds, originally showing SW-dipping axial planes locally rotated to a present gentle northward dip by later refolding (Barale et al., 2016a, compare with Malaroda, 1957), is partially displaced by SW-vergent low-angle thrust faults (d'Atri et al., 2016). This fold and thrust setting, which characterises the Monte La Piastra southern slope, where the Valdieri Marble quarries are located (Figs. 1c, 2, 3 is consistent at a regional scale and is well recorded also in the right side of the Gesso Valley near Entracque (see geological section A-A' in Barale et al., 2016a).

The above described S2 fold axial plane foliation is not continuous in the Valdieri Marble and it seems to have developed mainly in some stratigraphic levels, *e.g.* at the boundary between the recrystallised Marne Nere and the Desertetto Marble, particularly where the recrystallisation was not too intense (Fig. 15c). The S2 later became a slip-cleavage, since it acted as a multiple shear system to accomodate the shearing deformation which occurred in the later stages of F2 event (S2_sh in Fig. 14).

- The younger tectonic foliation which cross-cuts the Valdieri Marble is represented by a dm- to cm-spaced cleavage (S3 in Fig. 14) developed during the F3 tectonic event, where the shearing effect of E-W to NW-SE, high angle, reverse and strike slip faults occurring in both sides of Gesso valley (Malaroda, 1970; Barale et al., 2016a; d'Atri et al., 2016) is more intense. Where the fracture cleavage is closely spaced, fault breccias and cataclasites occur (Fig. 15d).

7 Radiometric data

7.1 Rationale and sampling strategy

In situ U-Pb isotope analyses were performed on seven thin sections (Fig. SM2 in the Supplementary Material) of Valdieri Marble samples in order to:

- date the formation of the marble bodies. Recrystallisation and neoblastesis affected Cretaceous sediments, and the crosscutting relationships between the regional foliations and the foliation developed within the marbles (see section 6) suggest that the formation of the marbles must have preceded the formation of the large scale F2 folds. Furthermore, preliminary petrographic observations made on samples collected in the Demonte-Aisone Zone (see Fig. 1b) (Malaroda, 2000), a few kilometres north of our study area, revealed that the shaly portions of the upper Eocene(?)-lower Oligocene Grès d'Annot are completely recrystallised, showing neoblastic mica minerals aligned to define a foliation which is in turn crosscut by the Alpine foliations. Field evidence thus just allows to place the marble formation between the early Oligocene and the late Oligocene (?) – early Miocene (?) (i.e. the ages of Alpine foliations). Uranium-Pb datings were designed to reduce as much as possible such time interval, thus providing robust age constraints indispensable to identify the geodynamic setting in which the marble formation occurred.
- verify the cogenetic relationships between calcite and silicate minerals aligned along the marble foliation, as suggested by the petrographic evidence (see section 5). Ablation spots were set off on pure calcite domains and on "mixed" fine-grained domains with both calcite and silicate minerals. Although silicate minerals made up less than 5% of the ablated material they have >10 times higher U concentrations as calcite. Hence, spot analyses of mixed domains should not plot on the same $^{207}Pb/^{206}Pb$ – $^{238}U/^{206}Pb$ arrays if not formed at the same time with calcite.
- understand if the marble and the veins that locally crosscut it are referable to the same event.

Samples were collected in order to be representative of all the recrystallised lithostratigraphic units (S. Lorenzo Marble, recrystallised Marne Nere, Desertetto Marble), of the different marble bodies (Cima Cialancia quarry, S. Lorenzo quarry, upper Desertetto valley), and of different rock domains (marble, veins, dolomite clasts) (Table 1).

7.2 Results

Uranium and Pb concentration of the 7 analysed samples are very variable and positively correlated, ranging from 0.007 to 18 ppm and 0.03 to 38 ppm, respectively. Spot analyses obtained over a small area (1.5 x 2 cm) commonly plot along a linear array in the $^{207}Pb/^{206}Pb$ vs $^{238}U/^{206}Pb$ space (Tera-Wasserburg diagram). This array is interpreted to be a mixture of initial common Pb and Pb that formed due to *in situ* decay of U since marble crystallisation. The age of formation is defined by the lower intercept with the Concordia. In five different samples the lower intercept ages are 32.4±5.0 Ma (CC8), 33.1±5.5 (MV200), 29.6±5.4 (MV19), 30.7±1.3 (MV28), 30.5±1.8 (MV47). In sample MV52 two distinct domains were analysed: a dolomite block yielded a lower intercept of 30.8±3.3 Ma, which is identical to the lower intercept age of a crosscutting vein of 30.0±2.9 Ma. Also in sample MV22, analyses from a dolomite block and from a crosscutting vein were within uncertainty indistinguishable, with a common lower intercept age of 31.3±2.0 Ma (Table 1).

The ages obtained on samples MV47 and MV28 show the smallest uncertainties; larger uncertainties of the other samples are usually related to the smaller variability of the U and Pb concentration and thus the limited spread in $^{238}U/^{206}Pb$ ratios (Table SM1 in the supplementary material). However, the ages are strongly internally consistent, and confirm that calcite recrystallisation, growth of neoblastic silicate minerals, development of a foliation and local opening and cementation of veins occurred in the same time interval, and thus can be referred to the same geological event. In figure 16the age of each sample with the respective 2σ error is graphically shown, and the weighted average of all analyses, corresponding to a common age interval between 30 and 31.6 Ma (early Oligocene), is reported.

8 Discussion

The above described geometric, stratigraphic, petrographic and geochemical features are here discussed in order to propose a new genetic process for the formation of the Valdieri

Marble. Moreover, the new U/Pb radiometric data presented in this paper give further constraints to interpret the tectono-stratigraphic evolution of the Maritime Alps.

8.1 Hydrothermal origin of the Valdieri Marble

The occurrence of the Valdieri Marble as isolated bodies within a carbonate succession which is not affected by neoblastic growth of silicates rules out any link with a regional metamorphic overprint.

Data and observations reported above strongly suggest, instead, that the Valdieri Marble originated by recrystallization of carbonate rocks of the Dauphinois Domain , as a consequence of infiltration of hydrothermal fluids in the early Oligocene. Evidence of fluid circulation is given by veins and carbonate-rich “pockets”, which are not affected by any recrystallisation, but are in equilibrium with the recrystallised host rocks. This not only implies equilibrium relationships between hydrothermal fluids and recrystallised host rocks, but also suggests that fluid circulation was coeval with the recrystallisation event. Within impure rock-types, recrystallisation of carbonate was accompanied by the neoblastesis of silicates, locally abundant and mainly represented by epidote, muscovite- to paragonite-rich mica, albite and K-feldspar. The typology of the newly-formed phases is strongly dependent on the local chemical composition of the system. The spatial transition between the sedimentary rocks and the corresponding recrystallised terms documents that the metamorphic reactions occurred during the marble formation. Approaching the Desertetto Marble from the Puriac Limestone the earlier transformation in the limestone is given by the recrystallisation of calcite and potassic mica, while quartz, K-feldspar and plagioclase - all of them of detrital origin - still survive as relics. With increasing intensity of transformation, the breakdown of feldspars occurs and new reactions (involving also quartz, which disappears as clastic grains, and calcite) produce further mica, together with epidote and chlorite. The resulting metamorphic assemblages are strongly variable, depending on microdomain composition (which determines, for instance, the stability of albite or paragonitic mica). Geothermometric estimates suggest (re-) crystallisation temperatures of ca. 350°C, therefore significantly

higher than the corresponding stratigraphic terms of the succession in the nearby areas, which never exceeded conditions of anchizone metamorphism.

8.2 Age of the hydrothermal event

U/Pb data from seven selected samples yielded within uncertainty identical ages consistent with the idea that Valdieri Marble formed during a short age interval between 30.0 and 31.6 Ma (early Oligocene). This perfectly agrees with the stratigraphic and structural observations, which constrain the Valdieri Marble formation between the early Oligocene and the late Oligocene (?) – early Miocene (?) (see section 7.1).

Radiometric data confirm the petrographic evidence suggesting that calcite recrystallisation, silicate mineral neoblastesis and development of a foliation occurred simultaneously. The age of the veins is identical to the age of the marbles: in agreement with the observed petrographic cogenetic relationships, it documents that opening and cementation of veins and formation of marble can be referred to the same hydrothermal event.

8.3 Geometry and kinematics of the Valdieri hydrothermal system

The Valdieri Marble is represented by marble bodies transitionally passing, over a distance of a few tens of metres, to slightly recrystallised carbonate rocks of the same stratigraphic levels, and are clearly affected by a syn-genetic tectonic foliation roughly parallel to the bedding (see section 6.2). It can be thus argued that the migration of hydrothermal fluids forming the Valdieri Marble occurred in a syn-tectonic context along low-angle shear zones roughly parallel with the sedimentary bedding. The latter had to be connected with high-angle master faults and fracture systems conveying the hydrothermal fluids and possibly rooted deeply in the basement.

The Valdieri Marble formed, in fact, within a major tectonic zone developed in the Maritime and westernmost Ligurian Alps (“Alpine SW Transfer” sensu d’Atri et al., 2016), resulting from the anastomosing branching of multiple fault systems (corresponding to the present ABF, DAZ and LiVZ deformation units, fig. 1b). The “Alpine SW Transfer” was active from

the early Oligocene to the early Miocene, transcurrent in the early Oligocene and mostly transpressional in late Oligocene and early Miocene. Some individual faults of the "Alpine SW Transfer" could have provided, in the early Oligocene, the pipe-like conduits (Sibson, 1987; see also Viola et al., 2005; Hensen et al., 2015) conveying hydrothermal fluids from the underlying continental basement. These fluids could then have migrated along low-angle shear zones (maybe local inter-stratal detachment surfaces within the Jurassic-Cretaceous succession) developed within some strike-slip duplexes affected by minor fracture density but significantly sheared. The mainly marly-clayey sediments of the Eocene to lower Oligocene Foreland Basin succession (*Globigerina* Marl and Grès d'Annot) acted as a cap, confining the hydrothermal fluids within the carbonate Mesozoic succession, and being only locally affected by recrystallisation (Fig. 17a).

When the regional convergent tectonics took place (F2 regional tectonic event sensu d'Atri et al., 2016), in late Oligocene, the fluid conduits were likely cut off by the low-angle faults related with the contractional deformation that caused the superposition of the Mesozoic Briançonnais units onto the Dauphinois ones and the overlying Eocene-lower Oligocene Foreland Basin successions (Malaroda, 1970; Gidon; 1972; Brizio et al., 1983; Maury and Ricou, 1983; Piana et al., 2009; Barale et al., 2016a, d'Atri et al., 2016). The early Oligocene strike-slip duplexes (and the marble bodies inside them) were then folded and displaced by the subsequent late Oligocene - early Miocene and further faulting stages (as shown in section 6.3.), up to their present structural setting (Fig. 17b).

8.4 Valdieri Marble hydrothermalism in the frame of the "Oligocene revolution"

The "Alpine SW transfer" was rooted in the fault and fracture network that since the Early Cretaceous hosted a huge hydrothermal circulation widespread for tens of km along the NE boundary of the Argentera Massif and adjoining sedimentary successions, as described by Barale et al. (2013, 2016b), and that also strongly controlled the tectono-sedimentary evolution of the External Briançonnais (Bertok et al. 2012) and Dauphinois–Provençal domains (Barale et al. 2017). Starting from the early Oligocene the "Alpine SW transfer"

acted as a regional transfer zone with significant left-lateral displacements (see fig. 19 in d'Atri et al., 2016) possibly accomodating, together with the coeval dextral transpression along the Periadriatic fault system (Handy et al. 2005) and the Simplon Line (Steck 2008), the 40-50° counterclockwise rotation of the Adria microplate and its westward indentation (Collombet et al. 2002; Handy et al. 2010; Dumont et al. 2011, 2012; Rolland et al. 2012).

The Valdieri Marble represents the first reported evidence of a localized heat flow in the early Oligocene along a segment of such regional transfer zone. It can be related to the early Oligocene thermal event, well documented in the Western and Central Alps (see discussion in Callegari et al. 2004; Beltrando et al. 2010; Garzanti and Malusà 2008) by multiple evidence such as the climax of the Periadriatic magmatism (dated at about 32 Ma, Giraud 1983, Venturelli et al. 1984, Baubron 1984, Davies & Von Blanckenburg 1995, Féraud et al. 1995; Kapferer et al. 2012), the record of a calc-alkaline magmatic event provided by volcanic clasts in the foreland basins (dated at about 32,8-30,5 Ma, e.g. Tavayannaz and Champsaur sandstones: Ruffini et al. 1995, 1997; Boyet et al. 2001; St. Lions and Clumanc conglomerates, Barrême basin: Schwartz et al. 2012; Saint-Antonin Conglomerate, Castellane Arc: Stanley 1980; Val d'Aveto-Petrignacola Formation: Mattioli et al. 2002), and the presence of lower Oligocene pyroclastic deposits in the Provence Foreland (Biot–Villeneuve-Loubet, Antibes, 32,5-30,8 Ma; Bellon 1981; Baubron 1984), as well as andesitic dykes (Giraud 1983) and small subvolcanic intrusive bodies of calc-alkaline affinity ("Estérellite de Drammont", 32.7±0.9 Ma; Giraud 1983, Féraud et al. 1995), and possibly connected to a lithospheric-scale geodynamic process (Rosenbaum et al. 2002; Vignaroli et al. 2008; Jourdan et al. 2013; Ring and Gerdes 2016).

Finally, the U/Pb datings between 30.0 and 31.6 Ma (early Oligocene) for the Valdieri Marble provide an absolute chronological constraint for the age of the main Alpine tectonic foliations and related main regional deformational events in the Provençal-Dauphinois and External Briançonnais domains of the Maritime Alps, which must be younger than early Oligocene.

Acknowledgments

The authors thank the Editor Wolf-Christian Dullo, the reviewers Roland Maas and Giancarlo Molli, whose useful suggestions and constructive criticisms really improved the manuscript. Elia Mulazzano, Debora Scanu, and Fabrizio Scarrone are kindly acknowledged for sharing field work. The research was funded by the University of Torino (ex 60% funds) and by the Italian CNR (National Research Council), Istituto di Geoscienze e Georisorse, unità di Torino. The Carbocalcio Cuneese Spa is kindly acknowledged for allowing access and sampling in the San Lorenzo quarry.

References

Abiad P, Bortolami G, Cancelmo C et al (1970) Carta geologica d'Italia, Foglio 90, "Demonte", II ed., Serv Geol It, Roma

Albanis Beaumont JF (1795) Travels through the Maritime Alps, from Italy to Lyons, across the Col de Tende, by the way of Nice, Provence, Languedoc, &c. with topographical and historical descriptions. Bensley, London

Barale L (2014) The Meso-Cenozoic stratigraphic successions adjoining the Argentera Massif: Stratigraphic, sedimentologic and diagenetic evidence of syndepositional tectonics (Unpublished doctoral dissertation). Torino: Università di Torino. Available online at https://tel.archives-ouvertes.fr/tel-01152641

Barale L, Bertok C, d'Atri A, Martire L, Piana F, Domini G (2016a) Geology of the Entracque–Colle di Tenda area (Maritime Alps, NW Italy). J. of Maps, 12 (*2*): 359–370

Barale L, Bertok C, Salih Talabani N, d'Atri A, Martire L, Piana F, Préat A. (2016b) Very hot, very shallow hydrothermal dolomitization: an example from the Maritime Alps (NW Italy–SE France). Sedimentology, 63 (7): 2037–2065

Barale L, Bertok C, d'Atri A, Martire L, Piana F. (2017) Stratigraphy, sedimentology and syndepositional tectonics of the Jurassic–Cretaceous succession at the transition between Provençal and Dauphinois domains (Maritime Alps, NW Italy). Rivista Italiana di Paleontologia e Stratigrafia, 123 (3): 355-378

Barelli V (1835) Cenni di statistica mineralogica degli Stati di S.M. il Re di Sardegna. Tipografia Fodratti, Torino

Baubron JC (1984) Volcanisme du Sud-Est de la France. In: Debrand-Passard S, Courbouleix S, Lienhardt MJ (eds) Synthèse géologique du Sud-Est de la France, Mem. BRGM, 125, pp 514–517

Bellon H (1981) Chronologie radiométrique (K-Ar) des manifestations magmatiques autour de la méditerranée occidentale entre 33 et 1 Ma. In: Wezel FC (ed) Sedimentary basins of mediterranean margins. Proc. Int. Conf. Urbino Univ., 20-22 October 1980, pp 341–360

Beltrando M, Lister GS, Rosenbaum G, Richards S, Forster MA (2010) Recognizing episodic lithospheric thinning along a convergent plate margin. The example of the Early Oligocene Alps. Earth Sci. Rev. 103 (3-4): 81-98

Bersezio R, Barbieri P, Mozzi R (2002) Redeposited limestones in the Upper Cretaceous succession of the Helvetic Argentera Massif at the Italy-France border. Eclogae geol Helv 95: 15-30

Boyet M, Lapierre H, Tardy M, Bosch D, Maury R (2001) Nature des sources des composants andésitiques des Grès du Champsaur et des Grès de Taveyannaz; implications dans l'évolution des Alpes occidentales au Paléogène. Bull Soc Géol France 172 (4): 487-501

Carraro F, Dal Piaz GV, Franceschetti B, Malaroda R, Sturani C, Zanella E (1970) Note Illustrative della Carta Geologica del Massiccio dell'Argentera alla scala 1: 50.000. Mem Soc Geol It 9: 557–663

Catella M (1965) Valdieri e le sue cave di marmo. Atti e rassegna tecnica della Società degli Ingegneri e degli architetti in Torino 19 (12): 660–663

Catella M (1969) Marmi Piemontesi. Cronache economiche CCIAA 313 (4): 51–64

Cathelineau M (1988) Cation site occupancy in chlorites and illites as a function of temperature. Clay Minerals 23: 471–485

Cordey F, Tricart P, Guillot S, Schwartz S (2012) Dating the Tethyan Ocean in the Western Alps with radiolarite pebbles from synorogenic Oligocene molasse basins (southeast France). Swiss J Geosci 105: 39–48

d'Atri A, Piana F, Barale L, Bertok C, Martire L (2016) Geological setting of the southern termination of Western Alps. Int J Earth Sci 105 (6): 1831–1858

Davies GR, Smith LB (2006) Structurally controlled hydrothermal dolomite reservoir facies: an overview. AAPG Bull 90: 1641–1690

Di Capua A, Vezzoli G, Groppelli G (2016) Climatic, tectonic and volcanic controls of sediment supply to an Oligocene Foredeep basin: The Val d'Aveto Formation (Northern Italian Apennines). Sedim Geol 332: 68-84

Dumont T, Simon-Labric T, Authemayou C, Heymes T (2011) Lateral termination of the north-directed Alpine orogeny and onset of westward escape in the Western Alpine arc: structural and sedimentary evidence from the external zone. Tectonics 30, TC5006, doi:10.1029/2010TC002836

Dumont T, Schwartz S, Guillot S, Simon-Labric T, Tricart P, Jourdan S (2012) Structural and sedimentary records of the Oligocene revolution in the Western Alpine arc. J Geodyn 56–57: 18–38

Fornaro M, Giuliani A, Lovera E (2005) Possibilità di riavvio di difficili coltivazioni di marmo alpino. Giornale di Geologia Applicata 2: 313–319

Franchi S (1926) Passaggi graduali a forme cristalline, calcescistose e marmoree, del Nummulitico e del Cretaceo fossiliferi, nelle Valli del Gesso e della Stura di Cuneo. Atti della Regia Accademia dei Lincei. Rendiconti 6 (3): 257–261

Frimmel HE (1997) Chlorite thermometry in the Witwatersrand Basin: constraints on the Paleoproterozoic geotherm in the Kaapvaal Craton, South Africa. J Geol 105, 601–615

Gerdes A, Zeh A (2006) Combined U-Pb and Hf isotope LA-(MC-) ICP-MS analyses of detrital zircons: comparison with SHRIMP and new constraints for the provenance and age of an Armorican metasediment in Central Germany. Earth Planet Sci Lett 249: 47–62

Gerdes A, Zeh A (2009) Zircon formation versus zircon alteration – New insights from combined U-Pb and Lu-Hf in-situ La-ICP-MS analyses of Archean zircons from the Limpopo Belt. Chem Geol 261(3–4): 230–243

Giglia G, Capponi G, Crispini L, Piazza M (1996) Dynamics and seismotectonics of the West-Alpine arc. Tectonophysics 267: 143–146

Giraud JD (1983) L'arc andésitique paléogène des Alpes occidentales. PhD Thesis, Université de Nice, 378 pp

Hansman RJ, Albert R, Gerdes A, Ring U (2018) Absolute ages of multiple generations of brittle structures by U-Pb dating of calcite. Geology 46 (3): 207-210

Incerpi N, Martire L, Manatschal G, Bernasconi S (2017) Evidence of hydrothermal fluid flow in a hyperextended rifted margin: the case study of the Err nappe (SE Switzerland). Swiss Jour Earth Sci 110 (2): 439-456Jourdan S, Bernet M, Schwartz S, Guillot S, Tricart P, Chauvel C, Dumont T, Montagnac G, Bureau S (2012) Tracing the Oligocene-Miocene evolution of the Western Alps drainage divide with pebble petrology, geochemistry, and Raman spectroscopy of foreland basin deposits. J Geo 120: 603–624

Jourdan S, Bernet M, Tricart P, Hardwick E, Paquette J, Guillot S, Dumont T, Schwartz S (2013) Short-lived, fast erosional exhumation of the internal western Alps during the late early Oligocene: constraints from geothermochronology of pro- and retro-side foreland basin sediments. Lithosphere 5 (2): 211-225

Kapferer N, Mercolli I, Berger A, Ovtcharova M, Fügenschuh B (2012) Dating emplacement and evolution of the orogenic magmatism in the internal Western Alps: 2. The Biella Volcanic Suite. Swiss J Geosci 105: 67–84

Handy MR, Babist J, Wagner R, Rosenberg C, Konrad-Schmolke M (2005) Decoupling and its relation to strain partitioning in continental lithosphere: insight from the Periadriatic fault system (European Alps). In: Gapais D, Brun JP, Cobbold PR (ed) Deformation mechanisms, rheology and tectonics: from minerals to the lithosphere. Book Series: Geological Society Special Publication 243: 249-276

Handy MR, Schmid SM, Bousquet R et al (2010) Reconciling plate-tectonic reconstructions of Alpine Tethys with the geological–geophysical record of spreading and subduction in the Alps. Earth-Sci Rev 102: 121–158

Kastner M (1971) Authigenic feldspars in carbonate rocks. Am Mineral 56: 1403–1442

Kranidiotis P, MacLean WH (1987) Systematics of chlorite alteration at the Phelps Dodge massive sulfide deposit, Matagami, Quebec. Econ Geol 82: 1898–1911

Malaroda R (1957) Studi geologici sulla dorsale montuosa compresa tra le basse Valli della Stura di Demonte e del Gesso (Alpi Marittime). Memorie degli Istituti di Geologia e Mineralogia dell'Università di Padova 20: 1–130

Malaroda R (1963) Les faciès à composante détritique dans le Crétacé autochtone des Alpes-Maritimes italiennes. Geol Rundsch 53: 41–57

Malaroda R (ed) (1970) Carta Geologica del Massiccio dell'Argentera alla scala 1:50.000. Memorie della Società Geologica Italiana 9

Malusà MG, Villa IM, Vezzoli G, Garzanti E (2011) Detrital geochronology of unroofing magmatic complexes and the slow erosion of Oligocene volcanoes in the Alps. Earth Planet Sci Lett 301: 324-336

Mendes da Costa E (1757) A Natural History of fossils. Davis and Reymers, London

Nicolis de Robilant SB (1786) Essai Géographique suivi d'une topographie souterraine, minéralogique, et d'une docimasie des États de S.M. en terre ferme. Memorie della Regia Accademia delle Scienze di Torino 6: 191–304

Piana F, Musso A, Bertok C, d'Atri A, Martire L, Perotti E, Varrone D, Martinotti G (2009) New data on post-Eocene tectonic evolution of the External Ligurian Briançonnais (Western Ligurian Alps). Ital J Geosci 128: 353–366

Piana F, Battaglia S, Bertok C, d'Atri A, Ellero A, Leoni L, Perotti E (2014) Illite (KI) and chlorite (AI) "crystallinity" indices as a constraint for the evolution of the External Briançonnais Front in Western Ligurian Alps (NW Italy). Ital J Geosci 133 (3): 445–454

Ring U, Gerdes A (2016) Kinematics of the Alpenrhein-Bodensee graben system in the Central Alps: Oligocene/Miocene transtension due to formation of the Western Alps arc. Tectonics 35: 1367–1391, doi: 10.1002/2015TC004085

Rosenbaum G, Lister GS, Duboz C (2002) Reconstruction of the tectonic evolution of the western Mediterranean since the Oligocene. J Virt Expl 8: 107-130

Ruffini R, Cosca MA, d'Atri A, Hunziker JC, Polino R (1995) The volcanic supply of the Taveyanne turbidites (Savoie, France): a riddle for Tertiary Alpine volcanism. Accademia Nazionale delle Scienze detta dei XL, Roma, Atti convegno Rapporti Alpi-Appennino, Peveragno: 359-376.

Ruffini R, Polino R, Callegari E, Hunziker JC, Pfeifer HR (1997) Volcanic clast-rich turbidites of the Taveyanne sandstones from the Thônes syncline (Savoie, France): records for a Tertiary postcollisional volcanism. Schweiz Mineral Petrogr Mitt 77 (2): 161-174

Roberts NMW, Rasbury E, Troy P, Randall R, Smith CJ, Horstwood MSA, Condon DJ (2017) A calcite reference material for LA-ICP-MS U-Pb geochronology. Geochemistry Geophysics Geosystems 18(7): 2807-2814

Schwartz S, Guillot S, Tricart P, Bernet M, Jourdan S, Dumont T, Montagnac G (2012) Source tracing of detrital serpentinite in the Oligocene molasse deposits from the western Alps (Barrême basin): implications for relief formation in the internal zone. Geol Mag 149(5): 841-856

Sinclair HD (1997) Tectonostratigraphic model for underfilled peripheral foreland basins: an Alpine perspective. GSA Bulletin 109: 324–346

Sismonda A (1833) Essai géognostique dans les deux vallées voisines de Stura et de Vinay. Memorie della Reale Accademia delle Scienze di Torino 36(1), 1–10

Sismonda A (1848) Notizie e schiarimenti sulla costituzione delle Alpi piemontesi. Memorie della Reale Accademia delle Scienze di Torino 9(2): 1–123

Stanley DJ (1980) The Saint-Antonin Conglomerate in the Maritime Alps; a model for coarse sedimentation on a submarine slope. Smithsonian Contributions to the Marine Sciences 5: 1–25

Vernet J (1967) Données récentes sur la tectonique du Massif de l'Argentera. Travaux du Laboratoire de Géologie de Grenoble 43: 217–243

Steck A (2008) Tectonics of the Simplon massif and Lepontine gneiss dome: deformation structures due to collision between the underthrusting European plate and the Adriatic indenter. Swiss J Geosci 101(2): 515-546

Vignaroli G, Faccenna C, Jolivet L, Piromallo C, Rossetti F (2008) Subduction polarity reversal at the junction between the western Alps and the Northern Apennines, Italy. Tectonophysics 450: 34–50

Walshe JL (1986) A six-component chlorite solid solution model and the conditions of chlorite formation in hydrothermal and geothermal systems. Econ Geol 81: 681–703

Whitney DL, Evans BW (2010) Abbreviations for names of rock-forming minerals. Am Mineral 95: 185–187

Zang W, Fyfe WS (1995) Chloritisation of the hydrothermally altered bedrock at the Igarape Bahia gold deposit, Carajas, Brazil. Miner Deposita 30: 30–38

Figure captions

Fig. 1. (a) Schematic geographical and geological map of the south-western Alps. **(b)** Geological sketch map of the NE side of the Argentera Massif between the lower Stura Valley and the Colle di Tenda, showing the main tectonics units and boundary faults. Modified from d'Atri et al. 2016. **(c)** Simplified geological map of the Desertetto Valley, showing the areal extension of the Valdieri Marble bodies (modified from Barale et al. 2016a and Malaroda 1970). The position of samples utilized for U/Pb geochronology, and the trace of geological section AA' of Fig. 3, are also shown.

Fig. 2. Panoramic view of the Desertetto Valley showing the position of Valdieri Marble quarries. Image taken from the western side of Monte Corno (coordinates 44°15'24.9"N, 7°23'37.8"E). The approximate position of geological section AA' of Fig. 3 is also shown.

Fig. 3. Geological section across the southern side of Monte La Piastra and the San Lorenzo quarry (see section trace in Fig. 1c).

Fig. 4. a: Puriac Limestone from the Entracque area, south-east of the main marble bodies (Fig. 1), under the microscope. The rock is mainly composed of microsparitic calcite and clastic quartz (Qtz), with very minor amount of clay material; neoblastic minerals are not observed. Plane polarized transmitted light; b, c: typical aspect of the San Lorenzo Marble in the field (b) and at the microscale (c; transmitted light, crossed polars). Cal: calcite, Ms: muscovite, Qz: quartz (mineral abbreviations from Whitney & Evans 2010); d: deformed dolostone clasts (yellowish) and micaceous domains (fine-grained grey portions) defining the foliation in the San Lorenzo Marble.

Fig. 5. Impure portions of the San Lorenzo Marble at the microscale (transmitted light; a, b and d in plane polarized light; c with crossed polars). a ÷ c: strongly deformed, thinly bedded structure, composed of alternating mm-thick domains with variable composition. d: foliated domain sharply interrupted by granoblastic calcite. Ab: albite, Cal: calcite, Kfs: K-feldspar, Ms: muscovite, Py: pyrite.

Fig. 6. a: stratigraphic boundaries (the succession is overturned) between white marbles (S. Lorenzo Marble), calcareous schists (recrystallised Marne Nere) and phyllosilicate-bearing marbles (Desertetto Marble) on the eastern side of the San Lorenzo quarry; b: porphyroclastic structure of the recrystallised Marne Nere under the microscope (transmitted light, crossed polars). Chl: chlorite; other abbreviations as in Figs. 4 and 5; c: a cutting surface in the Desertetto abandoned quarry: the marble shows a clast-supported breccia texture, composed of strongly flattened white marble portions embedded in a dark matrix; d: detail of the breccia texture of the Desertetto Marble.

Fig. 7. Desertetto Marble under the microscope (transmitted light microscopy, crossed polars). a: sharp contact between the granoblastic calcite (left) and the white mica + epidote domains (right). b: contact between micaceous domains (left) and granoblastic calcite domains is often marked by the interposition of a mm-thick rim composed of an intergrowth of calcite, white mica and chlorite. In these rims the white mica is rich in muscovite ($Mu_{0.79-0.90}$) and mostly occurs as randomly oriented, relatively coarse-grained flakes showing equilibrium relationships with both calcite and chlorite. c: syn-kinematic growth of epidote along a thin micaceous domain. The dark core of the epidote is represented by a thorium-rich allanite relic. d: post-kinematic epidote. The epidote porphyroblast statically overgrows a deformed foliation, defined by very fine-grained alignments of hematite. Ms-Pa s.s.: muscovite-paragonite solid solution.

Fig. 8. Mineral chemistry diagrams of epidotes (a) and white micas (b). a: composition of the epidote-group minerals from the Desertetto Marble shown in the epidote-allanite-clinozoisite triangle. 1: relict allanitic epidote within synkinematic epidote, 2: synkinematic epidote in the micaceous domains, 3: postkinematic epidote, 4: epidote in the carbonate “veins”, 5: allanitic epidote in partially recrystallised marble (eastern side of the San Lorenzo quarry). b: plot of the white mica composition in the Si vs. K/K+Na diagram. Desertetto Marble: 1: white mica defining the foliation in the micaceous domains, 2: randomly oriented Mu-rich mica associated with granoblastic calcite ± chlorite, 3: randomly oriented Mu-rich mica overgrowing the foliation, 4: Pa-rich mica at rim of the randomly oriented mica in the calcite-rich domains; 5: white mica in the calcite + epidote veins. 6: K-rich composition of the neoblastic mica in the Desertetto Marble affected by an intermediate degree of recrystallisation. The composition of detritic mica from the Puriac Limestone from Entracque area (Fig. 1) is also shown for comparison (7). San Lorenzo Marble: 8: muscovite from a calcite + quartz + altered Fe-carbonate + white mica cemented vein in a dolostone block in the lower part of the S. Lorenzo Marble; 9: muscovite from impure portions of the marble (see Fig. 5).

Fig. 9. Desertetto Marble, electron microprobe backscattered images. a: relics of allanitic epidote (REE-Ep) in neoblastic epidote (Ep). b: REE-enriched portions (REE-Ep, light grey) matching crystal zoning in metamorphic epidote suggesting that some REE redistribution occurred during the epidote growth.

Fig. 10. Plot of the chlorite composition from the Desertetto Marble in the classification diagram after Hey (1954). *Triangles*: oriented chlorite in the micaceous domains, *squares*: chlorite in equilibrium with randomly oriented white mica and calcite.

Fig. 11. Desertetto Marble, electron microprobe backscattered images. a: Mu-rich lepidoblasts (Ms) overgrowing the foliation in the micaceous domains. b: coarse-grained,

randomly oriented muscovitic mica (Ms) + calcite + chlorite (ripidolite) at rims of the foliated micaceous domains.

Fig. 12. Microscopic features of the Desertetto Marble in the eastern side of the San Lorenzo quarry, where the Puriac Limestone is affected by a moderate degree of recrystallisation. a: domains enriched in granoblastic calcite (Cal) enveloped by calcite + quartz intergrowths. Quartz commonly occurs as rounded grains or polycrystalline aggregates after clastic quartz (Qz). b, c: Neoblastic muscovite (Ms), oriented along a foliation, envelops relict domains mainly composed of clasts of detrital plagioclase and K-feldspar, partially sericitized. d: detrital titanite, monazite and tourmaline within a domain strongly enriched in neoblastic muscovite. The surrounding granoblastic calcite intergrowth contains clasts of detrital quartz. a, b, d: transmitted light, crossed polars. c: electron microscope backscattered image.

Fig. 13. a, b: hydrothermal veins in the S. Lorenzo quarry. A calcite-rich subvertical vein crosscutting the S. Lorenzo Marble (a), and a network of calcite + quartz ± Fe-carbonate ± muscovite veins in a dolostone block in the S. Lorenzo Marble (b); c: cutting face in a Desertetto Marble quarry. The foliated impure marble is crosscut by irregularly-shaped calcite ± epidote “pockets” (white). b: photomicrograph of a calcite – epidote “pocket”. Transmitted light, crossed polars.

.

Fig. 14 Conceptual graphical scheme representing the recurrent cross-cutting relations between the main tectonic features observed in the Desertetto-San Lorenzo quarry area: the main foliation (S2), developed as axial plane foliation of regional F2 folds, is locally dragged toward parallelism to late F2 reverse faults and it is subsequently displaced by syn-F3 reverse and strike-slip steep faults belonging to the northern prolongation of the Limone-

Viozene and Aisone deformation zones (sensu d'Atri et al. 2016). The older, syn-hydrothermal, shear folds are locally preserved within decimetre-thick domains roughly subparallel to the bedding (see inset and Fig. 15b).

Fig. 15. Foliation features in the Desertetto Marble, Desertetto quarries. a: in the breccia textured interval of the Desertetto Marble the alignement of lens-shaped, elongated marble portions defines the Sm foliation;b: Sm foliation in the Desertetto Marble is deformed by centimetre-sized similar folds, locally evolving, by shearing, into a slip cleavage (Sm_sh); c: the S2 foliation, locally recognizable in the Desertetto Marble, is represented by a mm- to cm-spaced dissolution cleavage; d: cataclasites related to the F3 tectonic event developed in the core of a sub-vertical fault zone crosscutting the Desertetto Marble.

Fig. 16. Diagram representing the measured radiometric U/Pb ages, with the corresponding 2σ errors, of samples listed in Table 1. The horizontal black line represents the mean age, obtained from the weighted average of all analyses.

Fig. 17. Two-step schematic sketch representing: a: the early Oligocene trascurrent stage during which hydrothermal fluids flowed up from the underlying crystalline basement along the main transcurrent faults and then migrated along low-angle shear zones developed within some strike-slip duplexes, giving rise to the Valdieri Marble; b: the late Oligocene transpressive stage during which the main fluid conduits were cut off by low-angle faults and marble bodies were displaced and folded. See text for further details.

Table 1. Position and lithostratigraphic units of the seven Valdieri Marble samples collected for U/Pb radiometric datings. Obtained ages are also given.

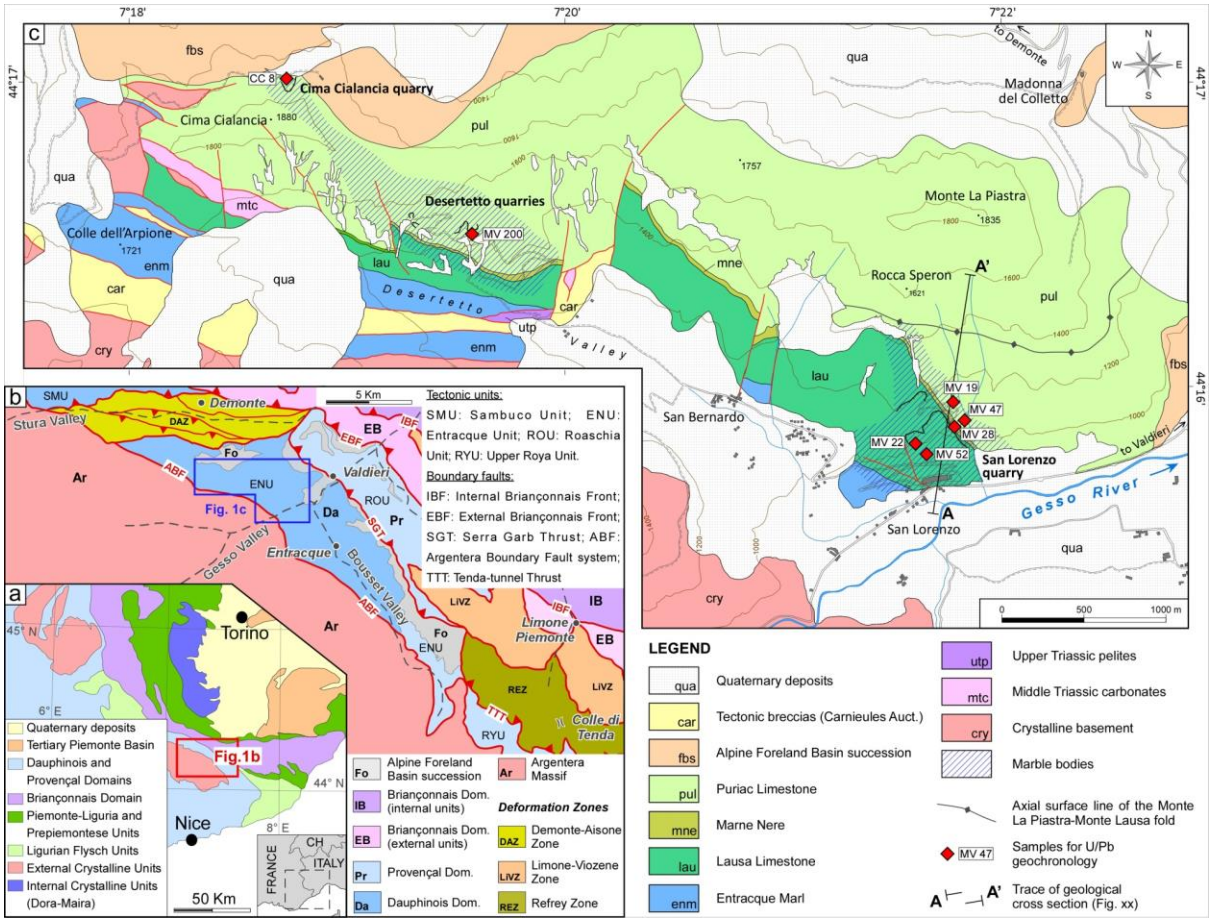
c
7°18'
7°20'
7°22'
44°17'
44°16'
fbs
CC 8
Cima Cialancia quarry
Cima Cialancia
1880
pul
qua
mtc
Colle dell'Arpione
1721
enm
car
cry
Desertetto quarries
MV 200
lau
Desertetto Valley
utp
enm
to Demonte
Madonna del Colletto
1757
Monte La Piastra
1835
mne
Rocca Speron
1621
A'
pul
car
lau
San Bernardo
MV 19
MV 47
MV 28
MV 22
MV 52
San Lorenzo quarry
to Valdieri
Gesso River
A
San Lorenzo
qua
cry
fbs
0
500
1000 m
b
SMU
Demonte
Stura Valley
DAZ
EB
IBF
EBF
Fo
Ar
ABF
ENU
Valdieri
ROU
Fig. 1c
Da
Pr
SGT
Entracque
Gesso Valley
Bousset Valley
5 Km
Tectonic units:
SMU: Sambuco Unit; ENU: Entracque Unit; ROU: Roaschia Unit; RYU: Upper Roya Unit.
Boundary faults:
IBF: Internal Briançonnais Front;
EBF: External Briançonnais Front;
SGT: Serra Garb Thrust; ABF: Argentera Boundary Fault system;
TTT: Tenda-tunnel Thrust
a
45° N
6° E
Torino
Ar
Fig.1b
44° N
8° E
Nice
50 Km
FRANCE
CH
ITALY
LIVZ
IB
Limone Piemonte
Fo
ENU
EB
REZ
LIVZ
TTT
RYU
Colle di Tenda
Quaternary deposits
Tertiary Piemonte Basin
Dauphinois and Provençal Domains
Briançonnais Domain
Piemonte-Liguria and Prepiemontese Units
Ligurian Flysch Units
External Crystalline Units
Internal Crystalline Units (Dora-Maira)
Fo Alpine Foreland Basin succession
IB Briançonnais Dom. (internal units)
EB Briançonnais Dom. (external units)
Pr Provençal Dom.
Da Dauphinois Dom.
Ar Argentera Massif
Deformation Zones
DAZ Demonte-Aisone Zone
LIVZ Limone-Viozene Zone
REZ Refrey Zone
LEGEND
qua Quaternary deposits
car Tectonic breccias (Carnieules Auct.)
fbs Alpine Foreland Basin succession
pul Puriac Limestone
mne Marne Nere
lau Lausa Limestone
enm Entracque Marl
utp Upper Triassic pelites
mtc Middle Triassic carbonates
cry Crystalline basement
Marble bodies
Axial surface line of the Monte La Piastra-Monte Lausa fold
MV 47 Samples for U/Pb geochronology
A A' Trace of geological cross section (Fig. xx)

Figure1

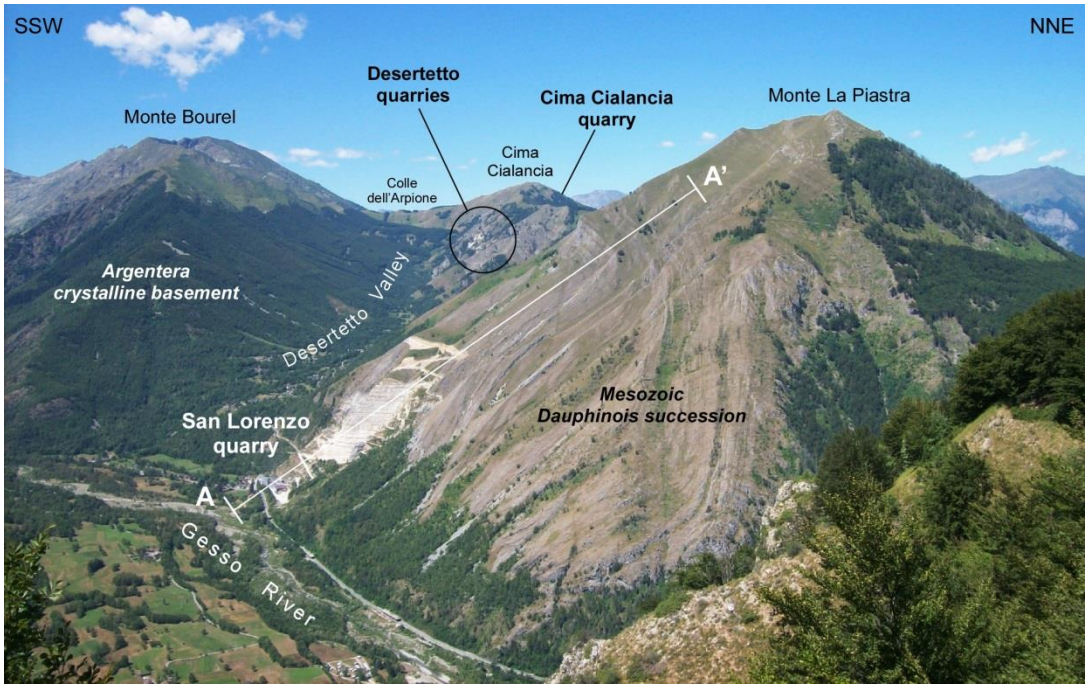
SSW
NNE
Desertetto
quarries
Cima Cialancia
quarry
Monte La Piastra
Monte Bourel
Cima
Cialancia
Colle
dell'Arpione
A'
Argentera
crystalline basement
Desertetto Valley
Mesozoic
Dauphinois succession
San Lorenzo
quarry
A
Gesso River

Figure 2

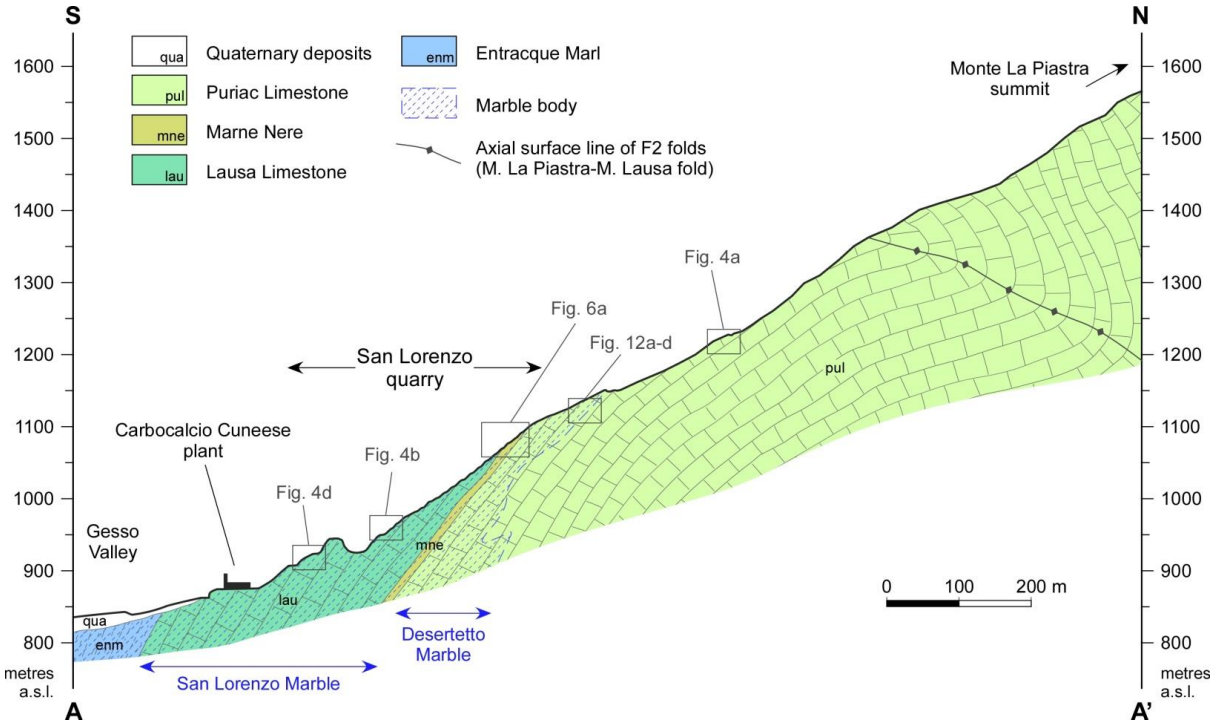
S
N
qua
Quaternary deposits
pul
Puriac Limestone
mne
Marne Nere
lau
Lausa Limestone
enm
Entracque Marl
Marble body
Axial surface line of F2 folds
(M. La Piastra-M. Lausa fold)
Monte La Piastra
summit
Fig. 4a
Fig. 6a
Fig. 12a-d
San Lorenzo
quarry
Carbocalcio Cuneese
plant
Fig. 4b
Fig. 4d
Gesso
Valley
pul
mne
lau
qua
enm
0
100
200 m
Desertetto
Marble
San Lorenzo Marble
1600
1500
1400
1300
1200
1100
1000
900
800
metres
a.s.l.
A
A'

Figure 3

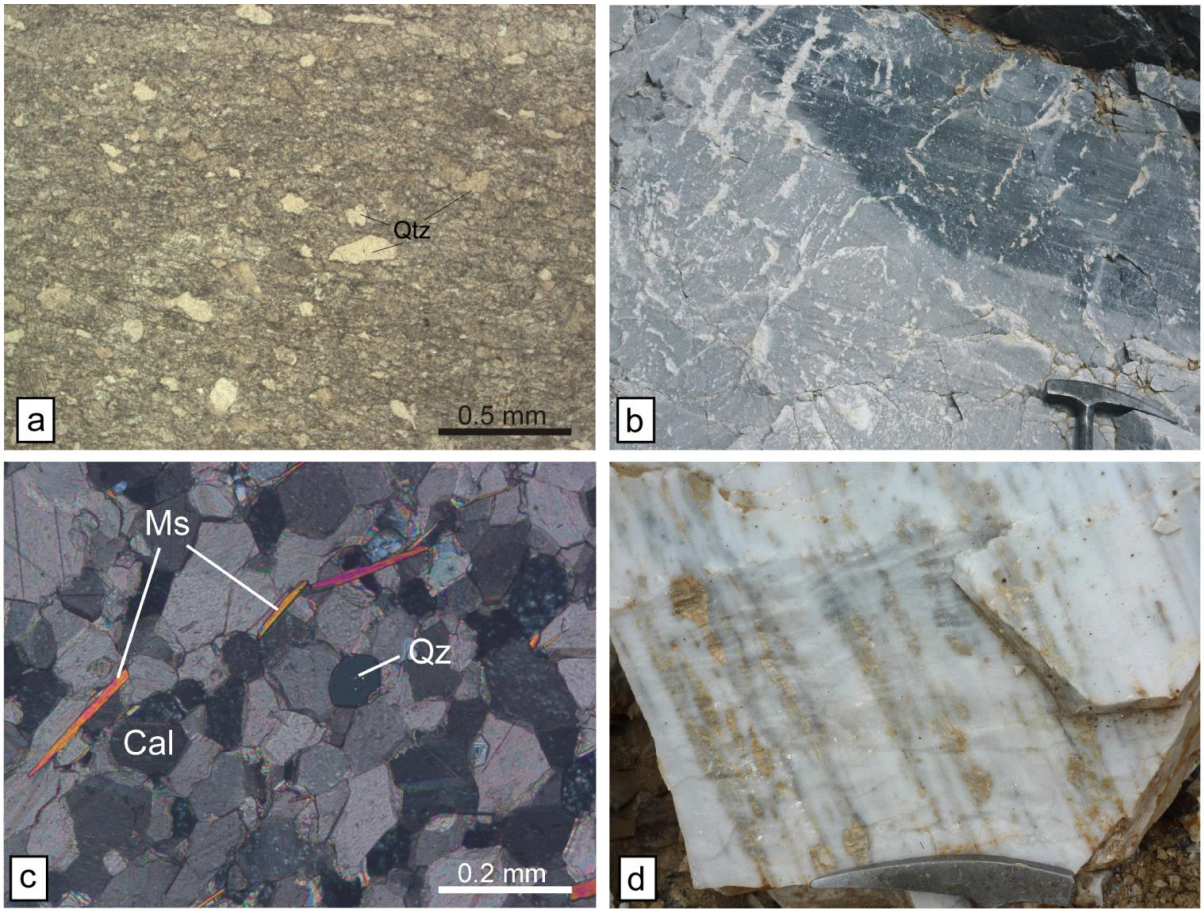

Figure 4

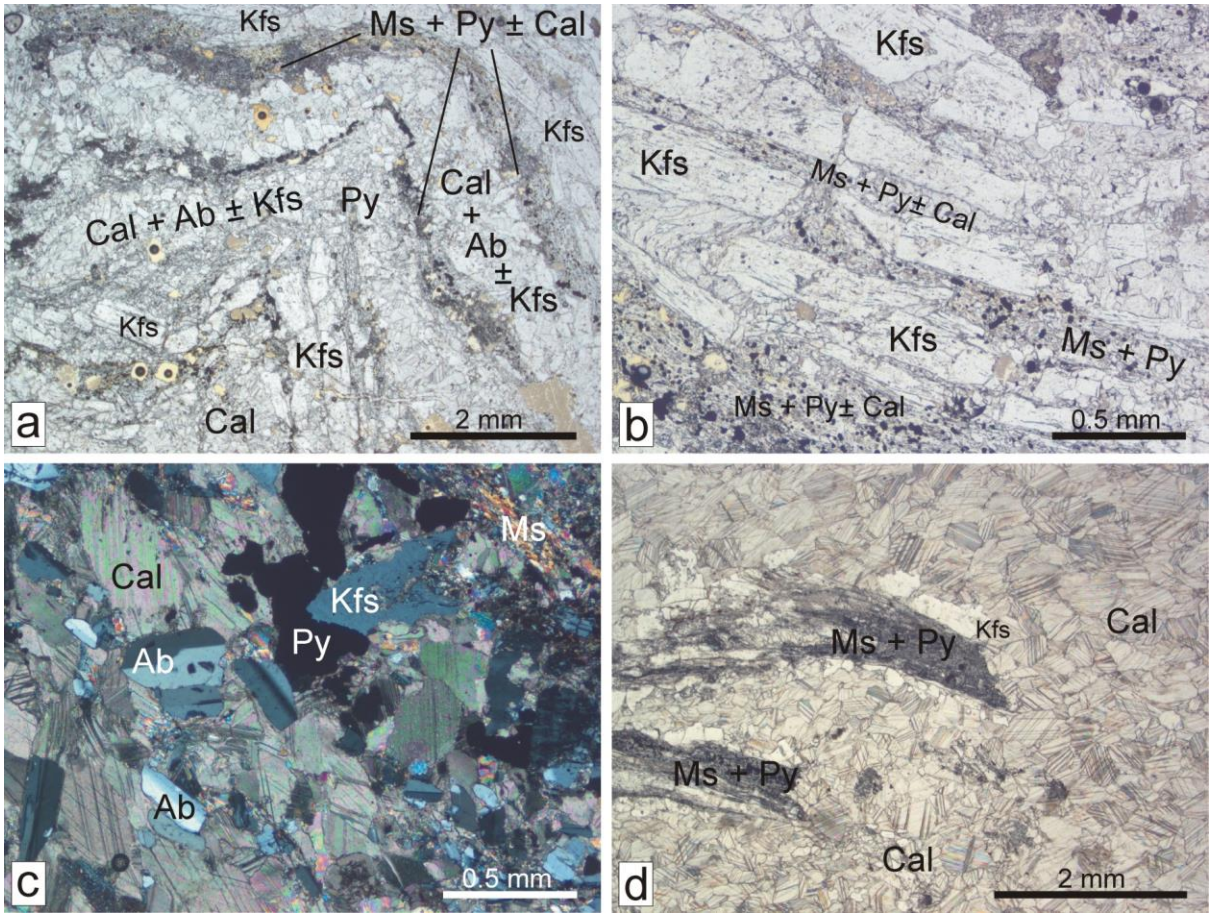
Kfs
Ms + Py ± Cal
Kfs
Cal + Ab ± Kfs
Py
Cal
+
Ab
±
Kfs
Kfs
Kfs
a
Cal
2 mm
Kfs
Kfs
Ms + Py± Cal
Kfs
Ms + Py
b
Ms + Py± Cal
0.5 mm
Ms
Cal
Kfs
Py
Ab
Ab
c
0.5 mm
Ms + Py
Kfs
Cal
Ms + Py
d
Cal
2 mm

Figure 5

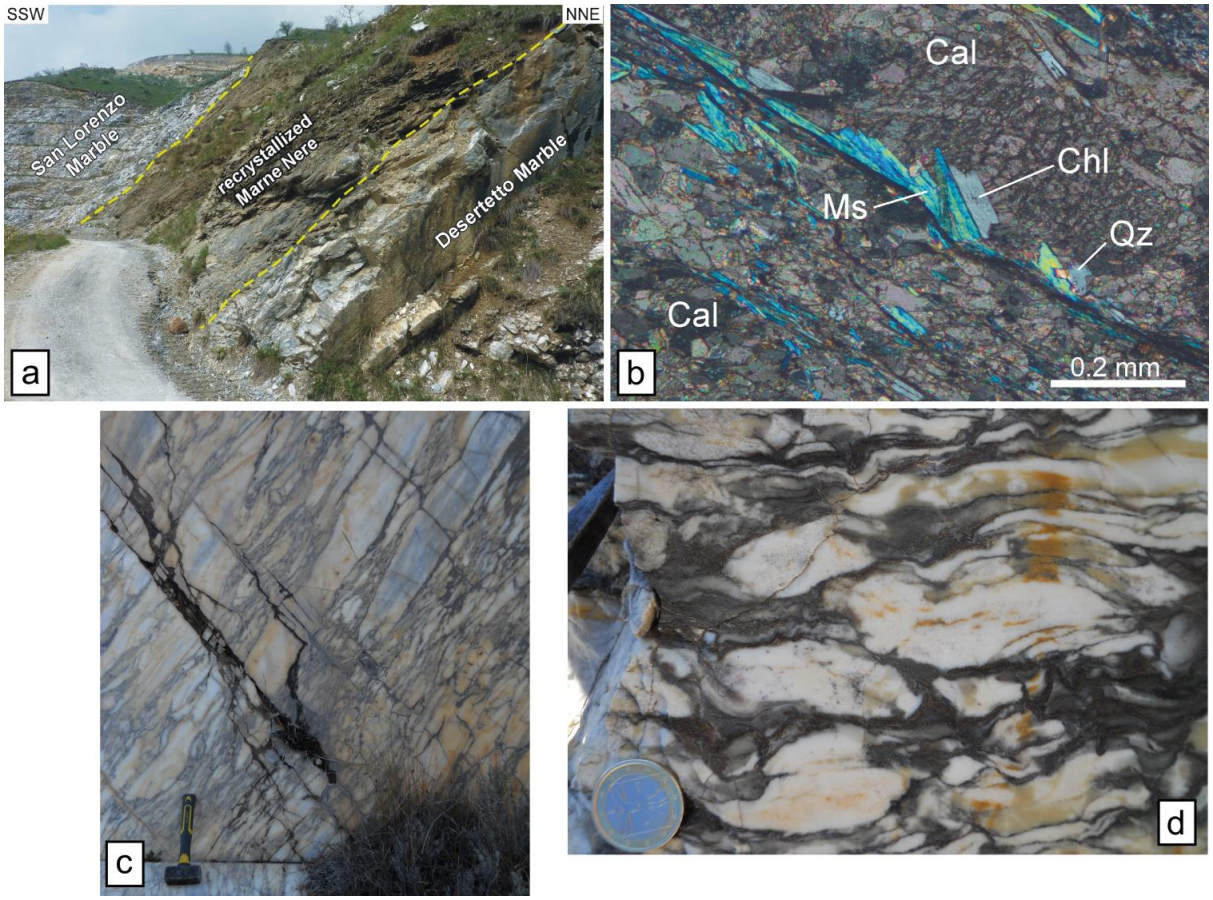
SSW
NNE
San Lorenzo Marble
recrystallized Marne Nere
Desertetto Marble
a
Cal
Chl
Ms
Qz
Cal
0.2 mm
b
c
d

Figure 6

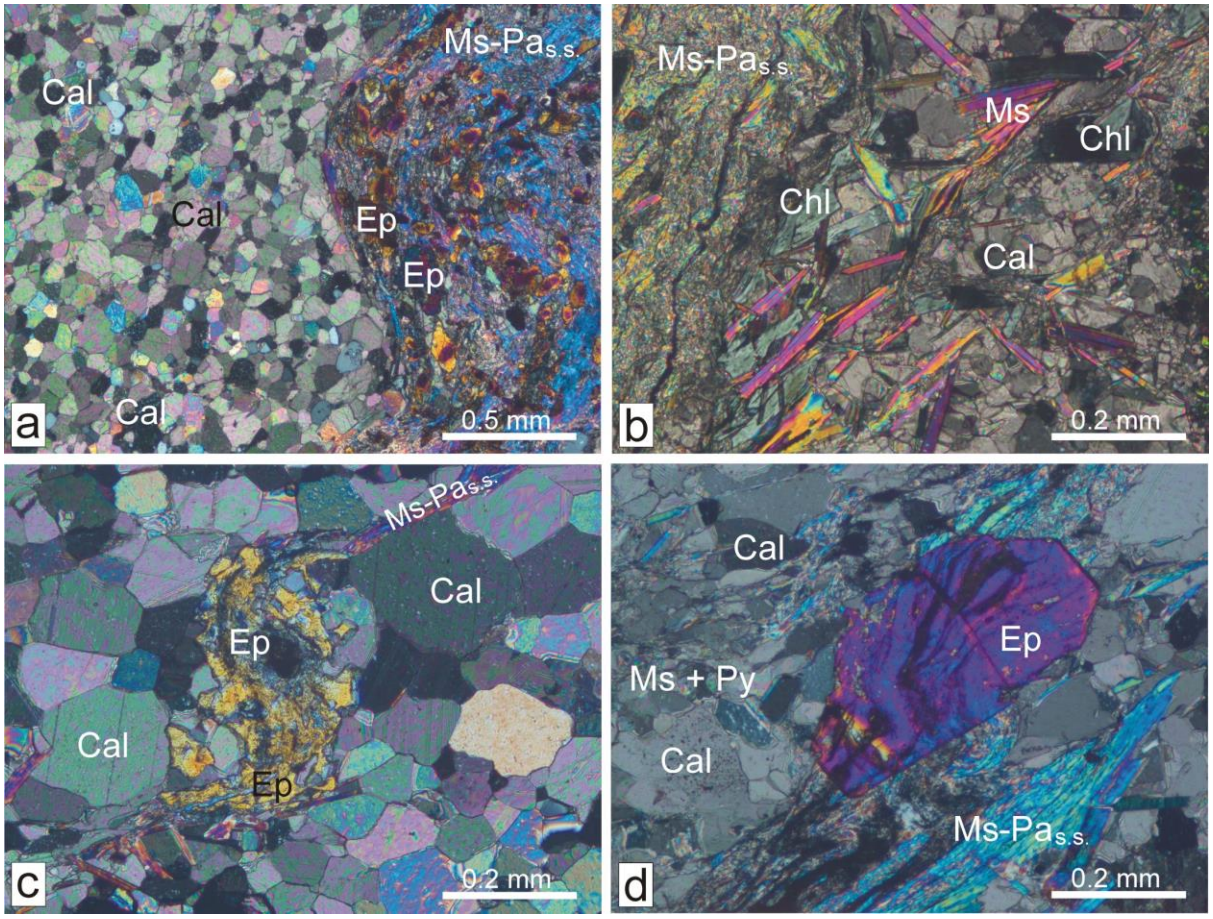
Ms-Pa$_{s.s.}$
Cal
Cal
Ep
Ep
Cal
a
0.5 mm
Ms-Pa$_{s.s.}$
Ms
Chl
Chl
Cal
b
0.2 mm
Ms-Pa$_{s.s.}$
Cal
Ep
Cal
Ep
c
0.2 mm
Cal
Ep
Ms + Py
Cal
Ms-Pa$_{s.s.}$
d
0.2 mm

Figure 7

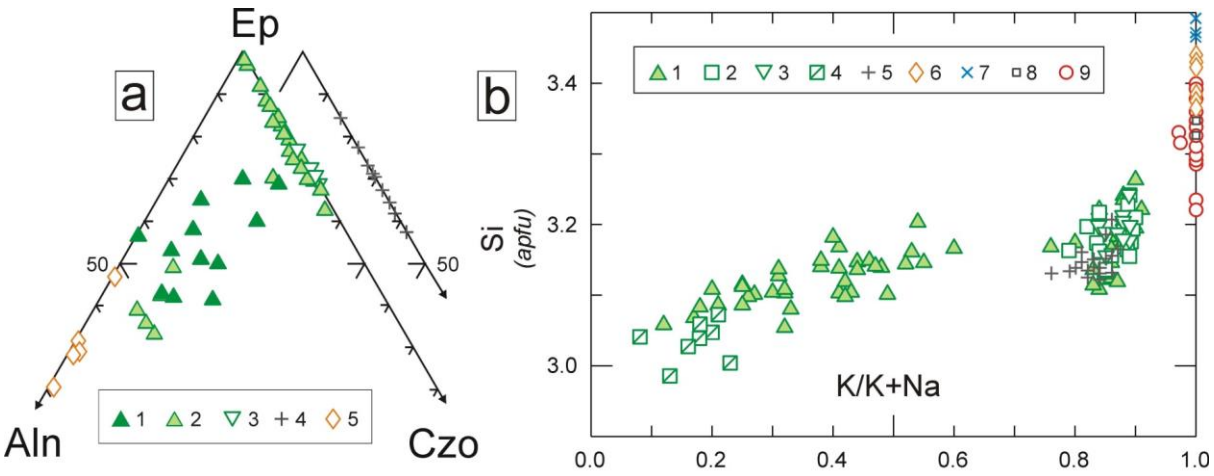
a
Ep
Aln
Czo
50
50
1 2 3 4 5
b
Si (apfu)
K/K+Na
3.4
3.2
3.0
0.0
0.2
0.4
0.6
0.8
1.0
1 2 3 4 5 6 7 8 9

Figure 8

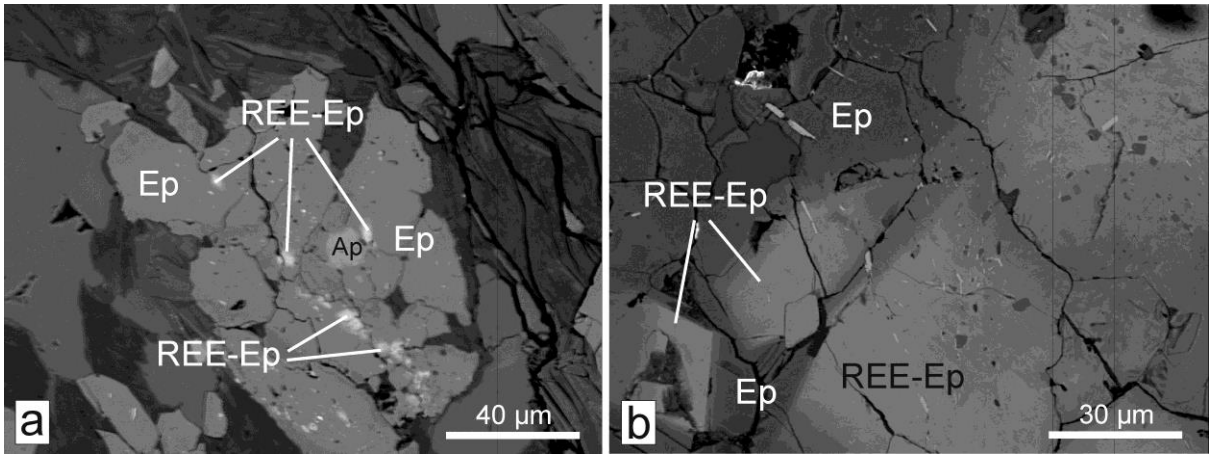

Figure 9

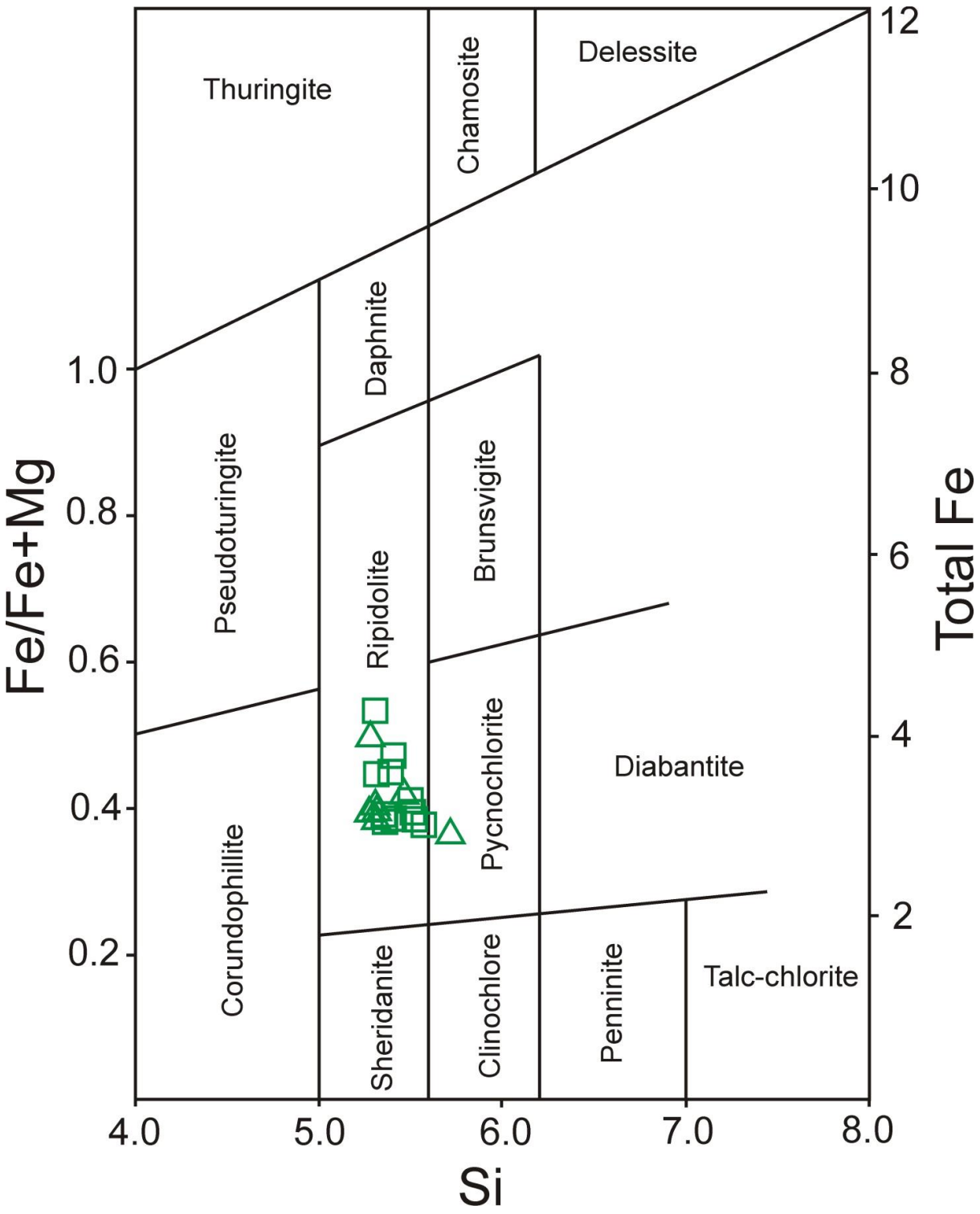
Thuringite
Chamosite
Delessite
Daphnite
Pseudoturingite
Ripidolite
Brunsvigite
Pycnochlorite
Diabantite
Corundophillite
Sheridanite
Clinochlore
Penninite
Talc-chlorite
Fe/Fe+Mg
Total Fe
Si
1.0
0.8
0.6
0.4
0.2
12
10
8
6
4
2
4.0
5.0
6.0
7.0
8.0

Figure 10

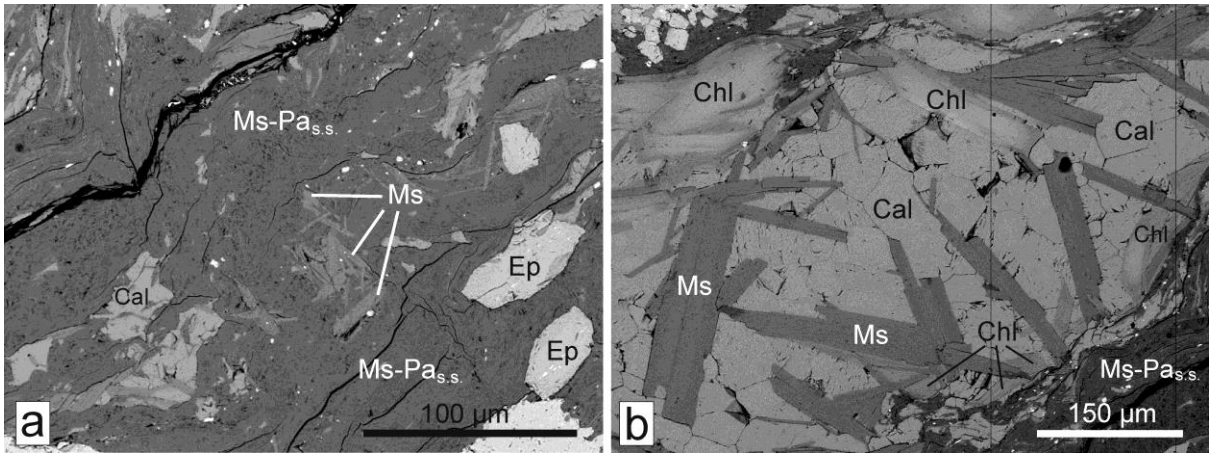
Ms-Pa$_{s.s.}$
Ms
Ep
Cal
Ep
Ms-Pa$_{s.s.}$
100 µm
a
Chl
Chl
Cal
Cal
Chl
Ms
Ms
Chl
Ms-Pa$_{s.s.}$
150 µm
b

Figure 11

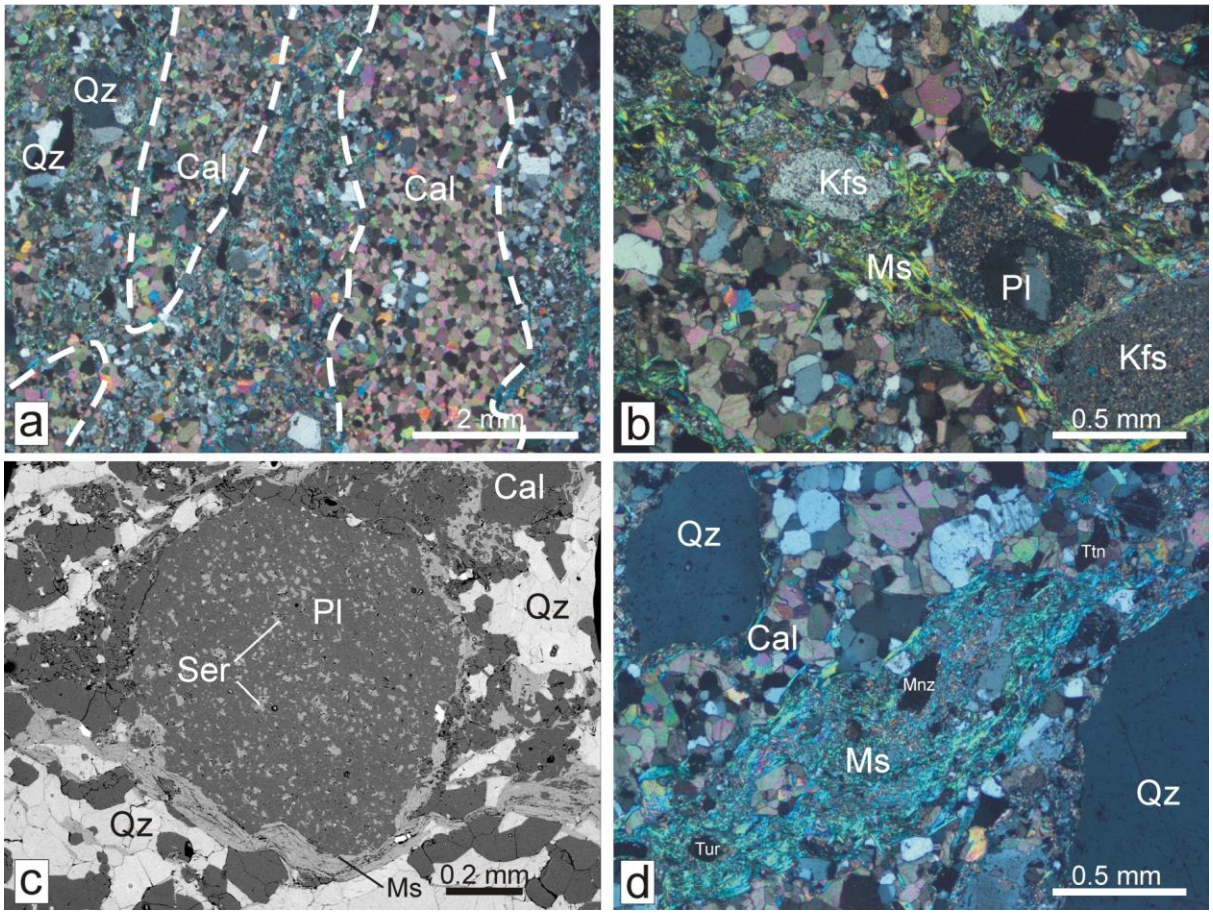
Qz
Qz
Cal
Cal
a
2 mm
Kfs
Ms
Pl
Kfs
b
0.5 mm
Cal
Pl
Qz
Ser
Qz
Ms
c
0.2 mm
Qz
Ttn
Cal
Mnz
Ms
Qz
Tur
d
0.5 mm

Figure 12

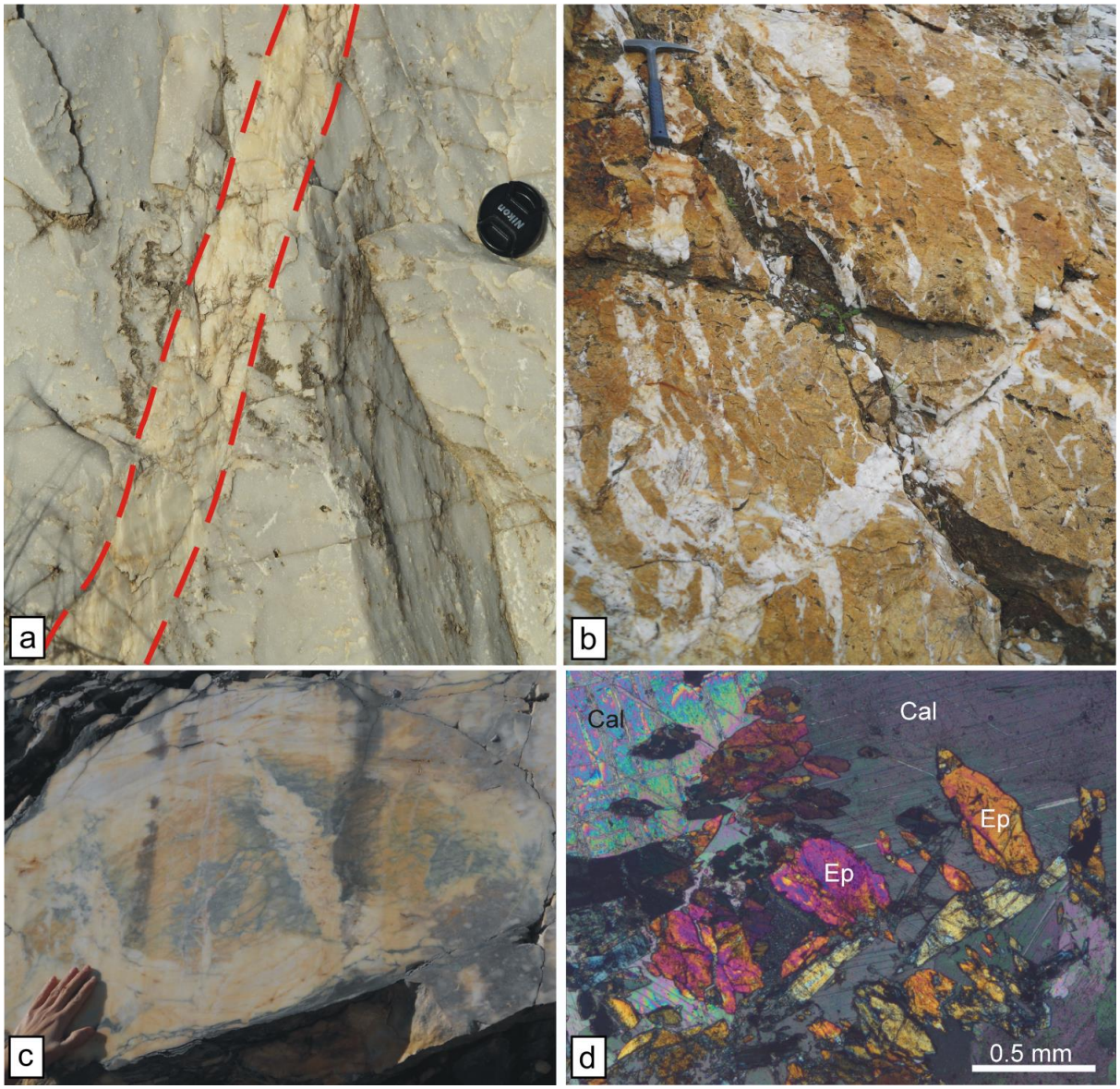

Figure 13

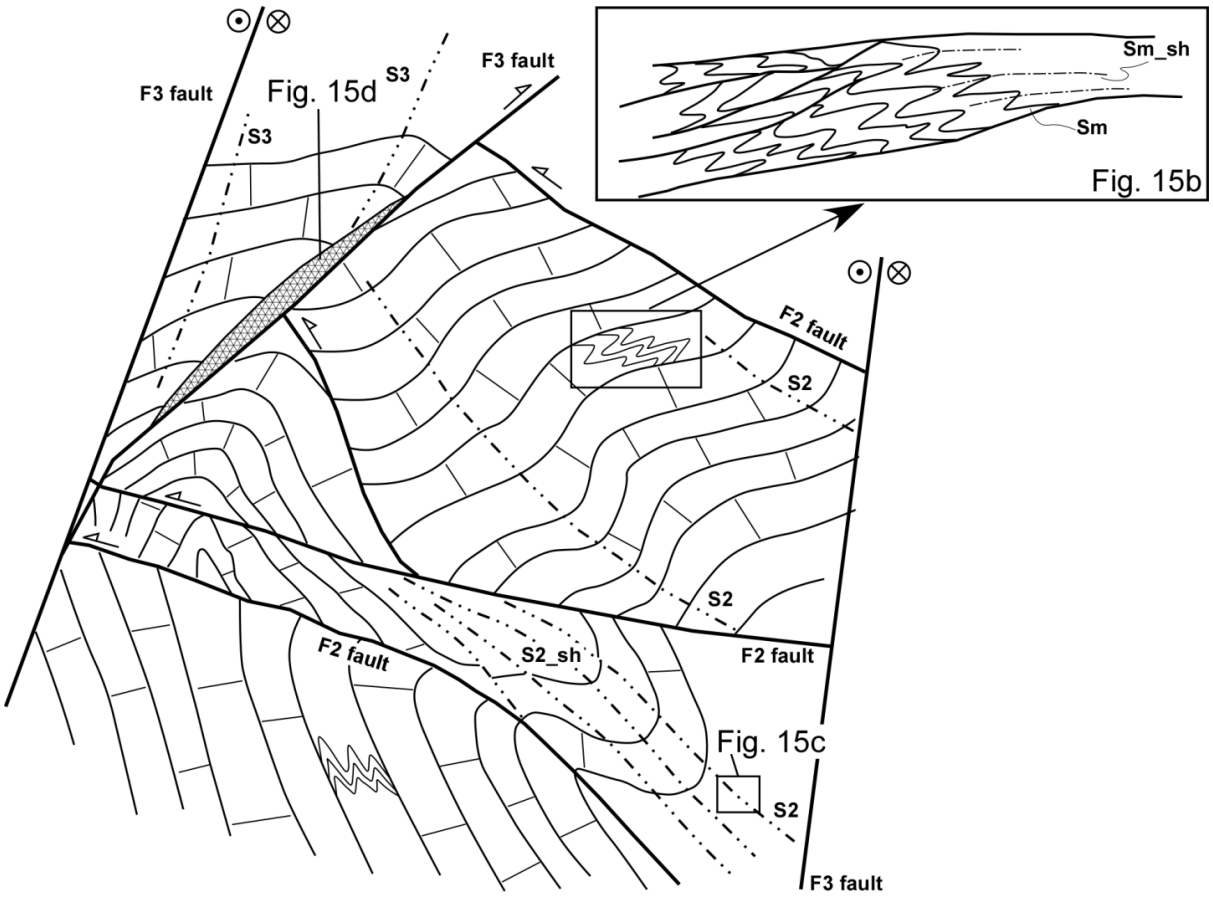
F3 fault
Fig. 15d
S3
S3
F3 fault
Sm_sh
Sm
Fig. 15b
F2 fault
S2
S2
F2 fault
S2_sh
F2 fault
Fig. 15c
S2
F3 fault

Figure 14

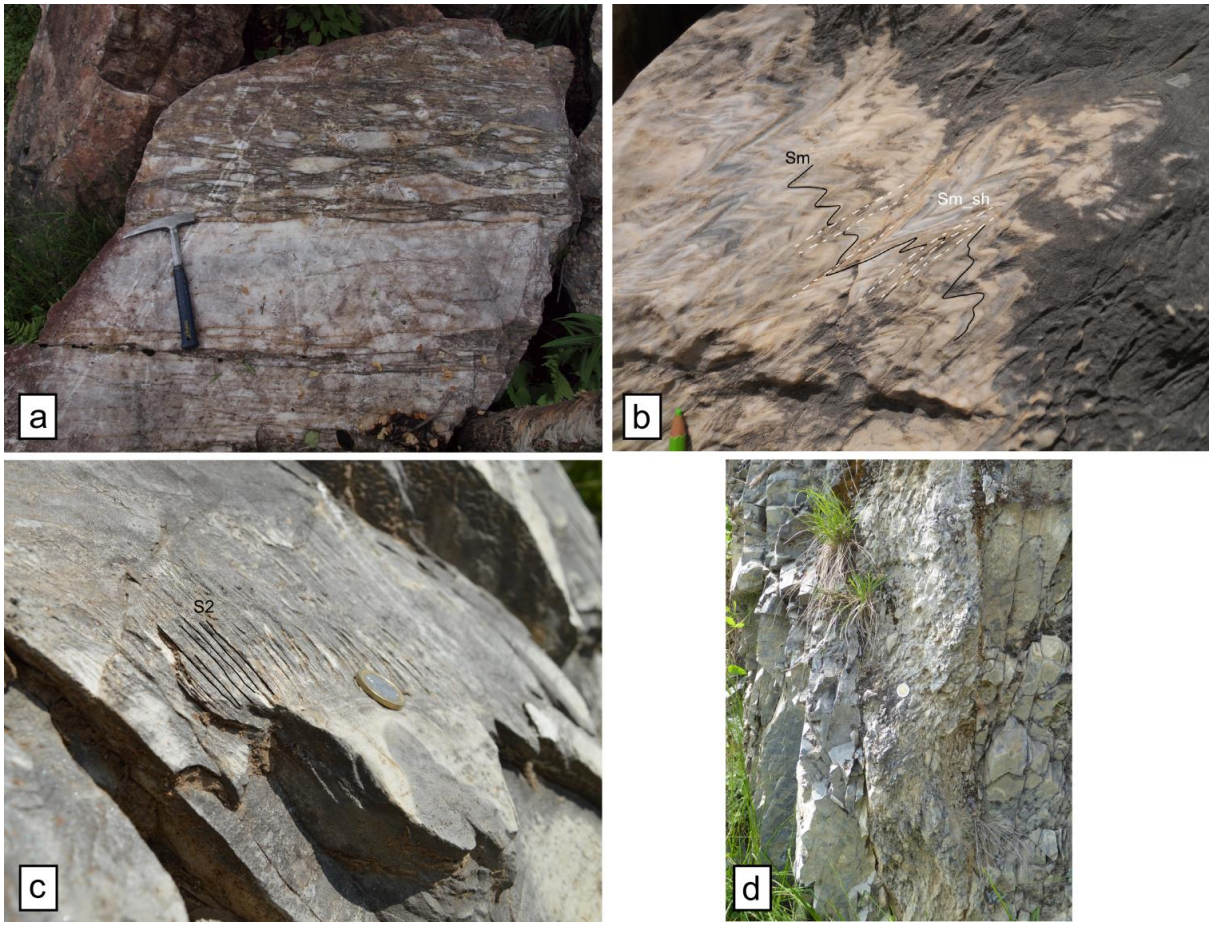

Figure 15

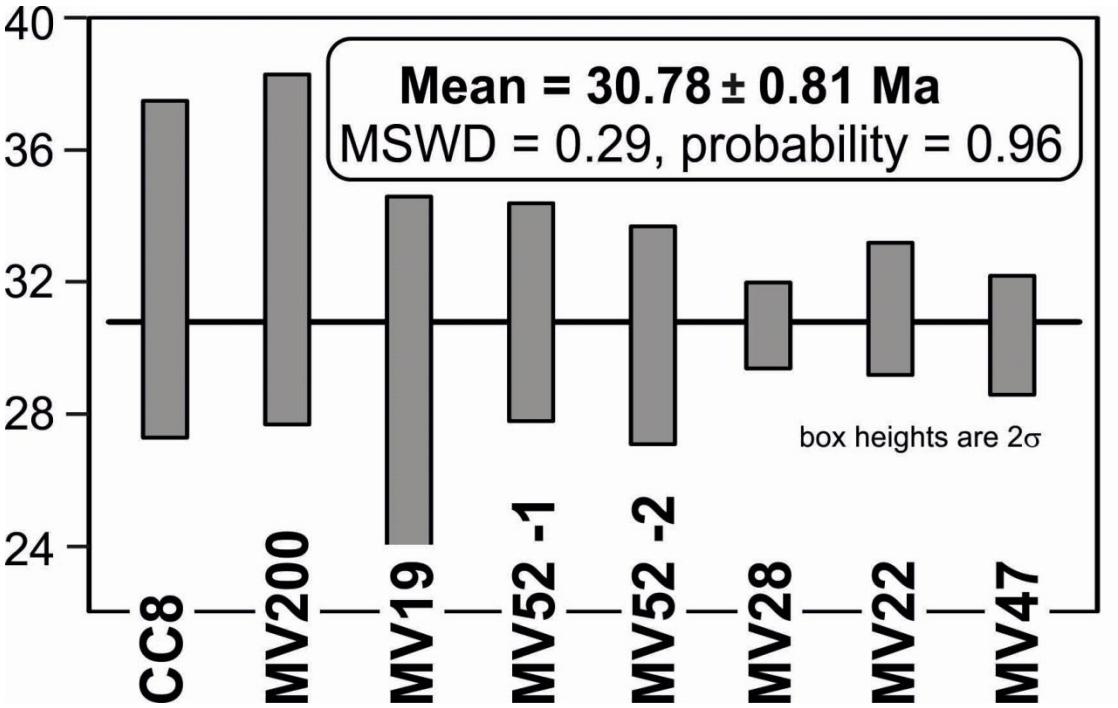
Mean = 30.78 ± 0.81 Ma
MSWD = 0.29, probability = 0.96
box heights are 2σ
40
36
32
28
24
CC8
MV200
MV19
MV52 -1
MV52 -2
MV28
MV22
MV47

Figure 16

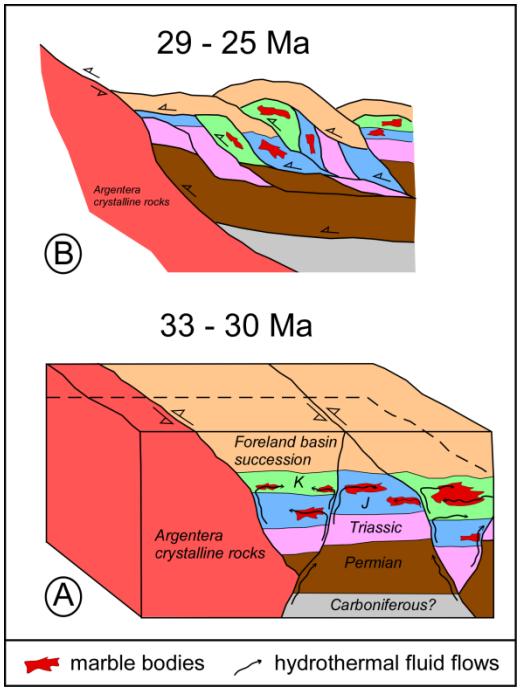
29 - 25 Ma
Argentera
crystalline rocks
B
33 - 30 Ma
Foreland basin
succession
K
J
Triassic
Argentera
crystalline rocks
Permian
Carboniferous?
A
marble bodies
hydrothermal fluid flows

Figure 17